OUKA
The University of Osaka
Institutional Knowledge Archive

Title	Recent research trends toward high-efficiency OPVs
Author(s)	Ie, Yutaka; Yamada, Hiroko
Citation	Journal of Photochemistry and Photobiology C: Photochemistry Reviews. 2025, 63, p. 100690
Version Type	VoR
URL	https://hdl.handle.net/11094/100977
rights	This article is licensed under a Creative Commons Attribution-NonCommercial-NoDerivatives 4.0 International License.
Note	

The University of Osaka Institutional Knowledge Archive : OUKA

https://ir.library.osaka-u.ac.jp/

The University of Osaka

Journal of Photochemistry & Photobiology, C: Photochemistry Reviews 63 (2025) 100690

Contents lists available at ScienceDirect

Journal of Photochemistry & Photobiology, C: Photochemistry Reviews

journal homepage: www.elsevier.com/locate/jphotochemrev

Invited Review

Recent research trends toward high-efficiency OPVs

Yutaka Ie [a,b,*], Hiroko Yamada [c,**]

[a] The Institute of Scientific and Industrial Research (SANKEN), Osaka University, 8-1 Mihogaoka, Ibaraki, Osaka 567-0047, Japan
[b] Innovative Catalysis Science Division, Institute for Open and Transdisciplinary Research Initiatives (ICS-OTRI), Osaka University, 2-1 Yamadaoka, Suita, Osaka 565-0871, Japan
[c] Institute for Chemical Research, Kyoto University, Gokasho, Uji, Kyoto 611-0011, Japan

ARTICLE INFO

Keywords:
Organic photovoltaics
Non-fullerene acceptors
Charge separation
Machine learning
Power conversion efficiency

ABSTRACT

Organic photovoltaics (OPVs) are at the forefront of renewable energy innovation due to their lightweight, flexible, and scalable properties. This review explores recent advancements in OPV researches, focusing on the intricate interplay of electronic and nuclear interactions that govern exciton behavior, charge separation, and transport mechanisms. By integrating theoretical insights with experimental findings, this review emphasizes the critical role of non-fullerene acceptors and advanced material design strategies in optimizing structure-property-function relationships. The application of machine learning is also highlighted as a transformative tool for correlating experimental data with device performance, enabling predictive frameworks for OPV development. Key breakthroughs in understanding charge carrier dynamics, interfacial interactions, and mobility relaxation provide a pathway for next-generation OPVs with enhanced power conversion efficiencies. These insights not only advance OPV technology but also hold promise for broader applications in organic optoelectronics.

1. Introduction

Organic photovoltaics (OPVs) have gained attention as promising next-generation energy sources owing to their advantages such as flexibility, light weight, large-area production, and compatibility with printing techniques [1,2]. The active layers of OPVs typically consist of donor (D) and acceptor (A), forming a bulk heterojunction (BHJ) structure. Although OPVs have achieved high power conversion efficiencies (PCEs) above 18 % [3,4], further innovations to increase PCEs are needed to make them suitable for social implementation. Typical OPVs convert sunlight into electric current through four main steps: (i) light absorption in the active layer, generating tightly bound excitons; (ii) exciton diffusion to D:A interfaces; (iii) exciton dissociation at the interface into charge-transfer (CT) states that further separate into free holes and electrons (i.e., charge-separated (CS) state); and (iv) charge transport through the donor and acceptor domains to the anode and cathode electrodes, respectively. Therefore, understanding and controlling these charge-carrier mechanisms are crucial for the development of OPVs. However, for the further enhancement of organic device performance, it is becoming increasingly important to understand excitons not only in terms of the conventional locally excited (LE) state but also with the contribution of CS and CT states. To distinguish these states from conventional excitons, the term "dynamic excitons" has recently been proposed [5].

In this review, we summarize recent trends toward highly efficient OPVs with a focus on key factors influencing excitons including CT (ranging from 0 % to 100 %), spin multiplicity, and D:A interactions (i.e., electronic coupling). This review consists of (1) introduction, (2) theoretical studies, (3) dye-sensitized solar cell (4) development of novel organic semiconductor materials for OPVs, (5) evaluation of OPV devices, (6) application of machine learning, and (7) conclusion.

2. Theoretical studies

In OPVs, the mechanism by which free electrons and holes are generated by overcoming the Coulomb attraction remains a subject of extensive debate. To investigate this process at the molecular level, Tamura and Burghardt conducted a combined electronic structure and quantum dynamics analysis, capturing the fundamental steps from exciton dissociation to free carrier generation at polymer-fullerene D:A heterojunctions [6]. Their calculations reveal that the experimentally observed efficient charge separation arises from two key effects. First,

* Corresponding author at: The Institute of Scientific and Industrial Research (SANKEN), Osaka University, 8-1 Mihogaoka, Ibaraki, Osaka 567-0047, Japan.
** Corresponding author.
E-mail addresses: yutakaie@sanken.osaka-u.ac.jp (Y. Ie), hyamada@scl.kyoto-u.ac.jp (H. Yamada).

https://doi.org/10.1016/j.jphotochemrev.2025.100690
Received 27 December 2024; Received in revised form 25 February 2025; Accepted 28 February 2025
Available online 4 March 2025
1389-5567/© 2025 The Authors. Published by Elsevier B.V. This is an open access article under the CC BY-NC-ND license (http://creativecommons.org/licenses/by-nc-nd/4.0/).

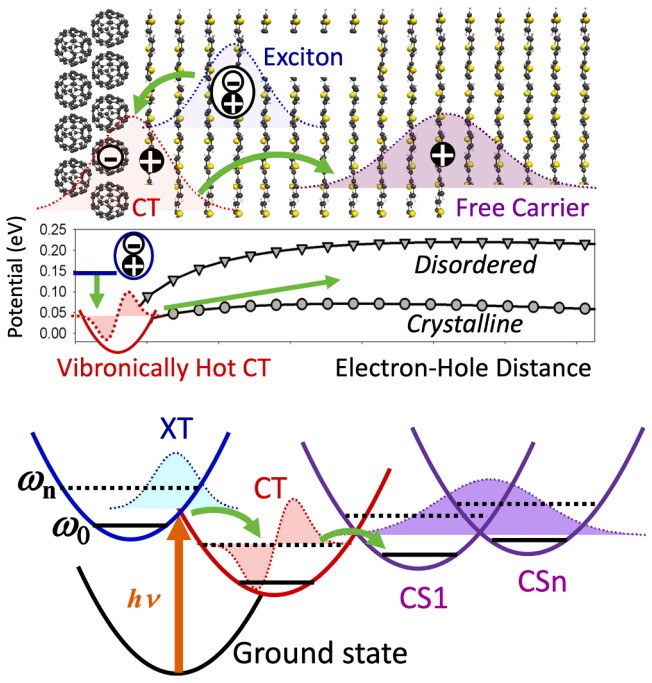

Fig. 1. Concept of charge separation enhanced by the vibronically hot CT mechanism. The excess energy of exciton leads to vibrational excitations in the CT state, and charge separation can occur before relaxation of the vibrational energy. Adapted with permission of [6]. Copyrights 2013 American Chemical Society.

charge delocalization significantly lowers the Coulomb barrier. Second, the vibronically hot nature of the charge-transfer state enhances charge dissociation beyond the barrier (Fig. 1). Together, these effects facilitate ultrafast charge separation, even at low-band-offset heterojunctions.

Exciton dissociation into free electron carriers is essential for efficient current generation in OPVs. Two mechanisms for this process are proposed: the "*Cool process*," where excitons relax to the CT state before thermally unbinding to the CS state, and the "*Hot process*," where excitons bypass the CT state and directly generate free charges at the D:A interface (Fig. 2) [7,8]. Muraoka et al. reported that the Frenkel exciton generated on the D side becomes a charge-transfer exciton at the interface, and the exciton size, that is, the electron-hole distance, correlates with the photoelectric conversion efficiency [9]. The charge-transfer exciton at the initial stage of formation is considered to be a weakly bound electron-hole polaron pair, and the process of its dissociation into a free electron polaron and a hole polaron without relaxation to the CT state is predicted to correspond to the *Hot process*. Therefore, the selection factor for the *Cool process* and *Hot process* is a non-adiabatic process owing to vibrational interactions in the initial charge-transfer excitonic state.

No consensus has been reached regarding the exact mechanism of CS. Yu et al. suggested that changes in the dipole moment during the intramolecular charge transfer of donor molecules ($\Delta\mu_D$) are important for efficient charge generation, and that the internal dipole moment along the polymer chain is important for the maintenance of pseudo-charge transfer [10]. However, the role of dipole moment variation in efficient charge generation is unclear. In this situation, identifying descriptors to quantify the effectiveness of CS is necessary for further development of OPVs. Muraoka et al. focused on the amount of charge transfer (ΔQ), charge transfer distance (d_{CT}), and change in dipole moment between the ground and excited states of the D:A complex ($\Delta\mu_{D:A}$). These descriptors can be easily calculated using the widely used density functional theory (DFT) and time-dependent DFT (TD-DFT), and the correlation between ΔQ, d_{CT} [11,12], $\Delta\mu_{D:A}$ and the CS efficiency can be numerically determined. A heterojunction model using three π-conjugated polymers (PTB7, PTB1, and PTBF2) as donors and [6,6]-phenyl-C_{71}-butyric acid methyl ester ($PC_{71}BM$) as an acceptor was analyzed for CT characteristics (Fig. 3) [9]. The polymers exhibited different short-circuit current densities (J_{SC}), external quantum efficiency (EQE), with PTB7 having the highest J_{SC} (Table 1). Calculations revealed that charge transfer between the donor and acceptor decreased as J_{SC} decreased. Although ΔQ was similar across all polymers, d_{CT} of PTB7:$PC_{71}BM$ was significantly longer than that of PTBF2:$PC_{71}BM$ and PTBF2:$PC_{71}BM$, correlating with its higher J_{SC} and more effective CS. These results indicate that the design of D:A interfaces with large values of ΔQ, d_{CT}, and $\Delta\mu_{D:A}$ is a prerequisite for developing high-efficiency polymer:$PC_{71}BM$ solar cells.

To elucidate the dynamic processes of excitons at the D:A interface in OPVs based on a nonfullerene acceptor (NFA) (Fig. 4), Muraoka et al. elucidated the role of oscillatory interactions in the CT excitonic state, J_{SC} and electron-hole recombination in the selection of *Cool* and *Hot processes* in the D:A system (PTB7:BTA*x* (*x* = 1, 3)) using TD-DFT [13]. Fig. 5 shows the potential surfaces of the ground and excited states of D:A. The vertical transition from the ground-state A_G to the excited-state A_E produces D:A local or CT-type excitations in the D:A; A_E is a Frenkel-type exciton produced in the donor, corresponding to a Wannier-type exciton at the D:A interface; and B_E is a structurally relaxed CT state with a pair of electron and hole polarons. The charge

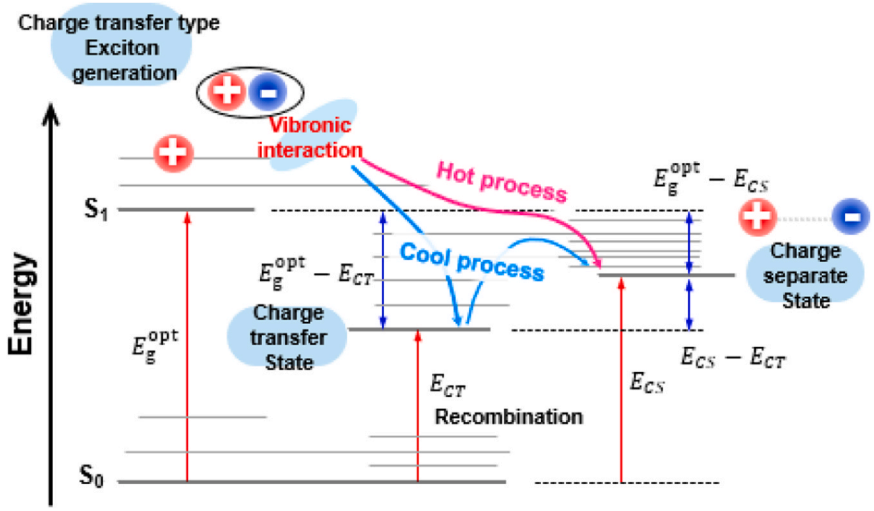

Fig. 2. Energetics of relevant states at D:A interfaces.

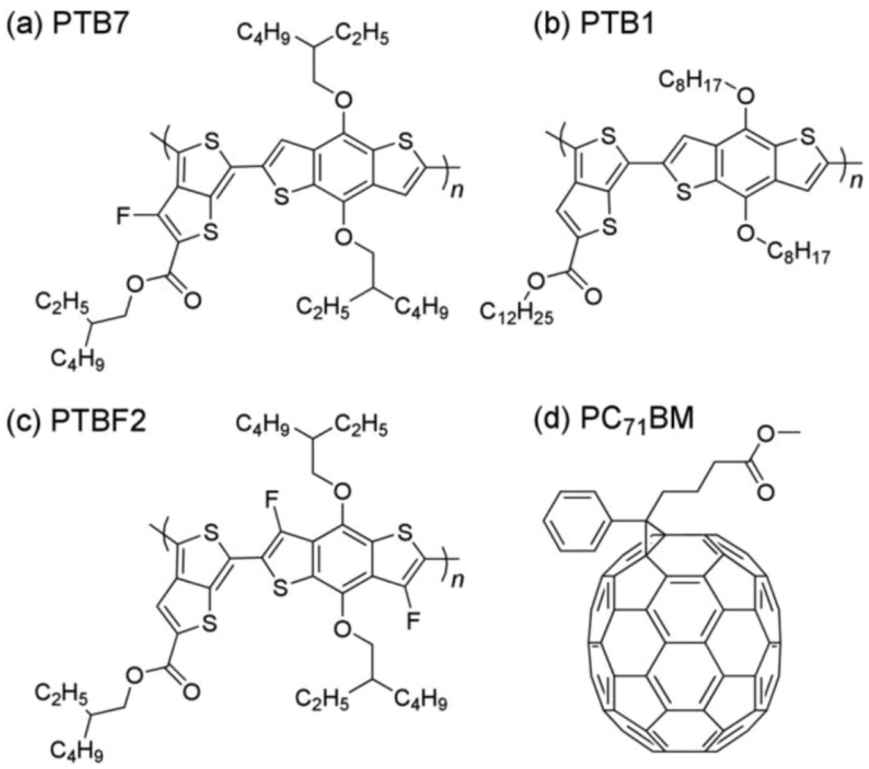

Fig. 3. Chemical structures of (a) PTB7, (b) PTB1, (c) PTBF2 and (d) $PC_{71}BM$. Reprinted with permission of [9]. Copyrights 2018 The Royal Chemical Society.

Table 1
Comparison of J_{SC} and EQE measured experimentally with key charge transfer parameters, including the amount of transferred charge (ΔQ), charge transfer distance (d_{CT}), and the variation of the dipole moments between the ground and excited states of the D/A complexes ($\Delta\mu_{D/A}$). Data are presented for PTB7/$PC_{71}BM$, PTB1/$PC_{71}BM$, and PTBF2/$PC_{71}BM$ systems. Reprinted with permission of [9]. Copyrights 2018 The Royal Chemical Society.

	PTB7/$PC_{71}BM$	PTB1/$PC_{71}BM$	PTBF2:$PC_{71}BM$
J_{SC} (mA/cm^2)	14.5	14.1	11.1
EQE (%)[a])	65–70	55–60	~45
ΔQ	0.552	0.497	0.467
d_{CT} (Å)	1.020	0.418	0.202
$\Delta\mu_{D:A}$ (Debye)	2.707	0.999	0.453

a) EQEs at absorption wavelengths of the polymer donors from 600 to 675 nm.

transfer distance in the CT (B_E) state is longer in PTB7:BTA1 because of the CT relaxation in B_E, which is vertically excited from the A_G through the A_E and then relaxed. This phenomenon indicates that the exciton size is larger because of the weaker Coulomb force, indicating that BTA1 is more likely to become a free carrier when relaxed to the CT state. Thus, the structural relaxation to the CT state may promote the formation of free carriers by the thermal dissociation of excitons.

To analyze the dynamic process in the CT state, Franck-Condon simulations were used to obtain the Huang-Rhys (HR) factor [14] and assess the nonadiabatic process owing to the vibronic interaction. As shown in Fig. 6, in the $B_E \rightarrow S_0$ process, PTB7:BTA1 exhibited a stronger HR factor at low frequencies, whereas PTB7:BTA3 exhibited a stronger HR factor at high frequencies. In the $B_E \rightarrow S_0$ process, PTB7:BTA1 has in-plane and out-of-plane low-frequency side-chain vibrations of the acceptor, whereas PTB7:BTA3 shows strong in-plane vibrations of the donor. According to Fermi's golden rule, lower frequencies increase the density of states and thus the higher the transition probability, that is, the more likely non-adiabatic processes. Thus, according to the HR analysis, the A_E in PTB7:BTA1 is more prone to nonradiative recombination, resulting in a lower J_{SC} compared to PTB7:BTA3. This suggests that PTB7:BTA1 underwent nonradiative relaxation in the CT state, contributing to its higher open-circuit voltages (V_{OC}) loss.

Computational simulations, particularly non-adiabatic molecular dynamics (NA-MD), are valuable for analyzing exciton dynamics in OPVs. NA-MD combines quantum mechanical treatment of excited states with classical mechanics for nuclear dynamics, but faces high computational costs, especially for large molecular systems of OPVs (~10^2 atoms). Uratani et al. developed a new NA-MD technique to treat

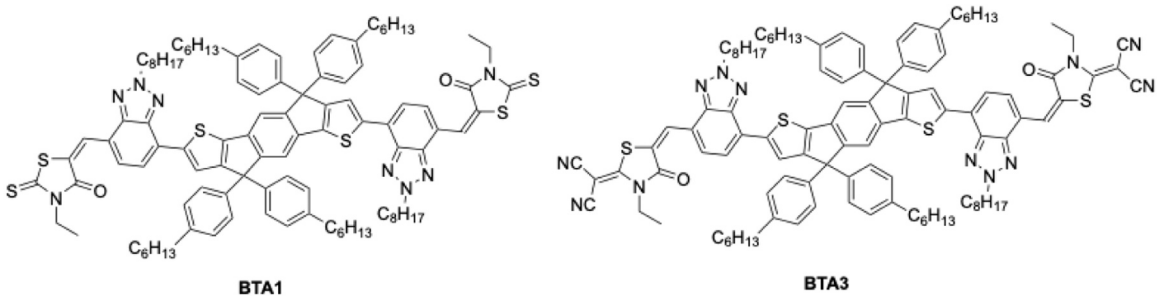

Fig. 4. Chemical structures of BTA1 and BTA3.

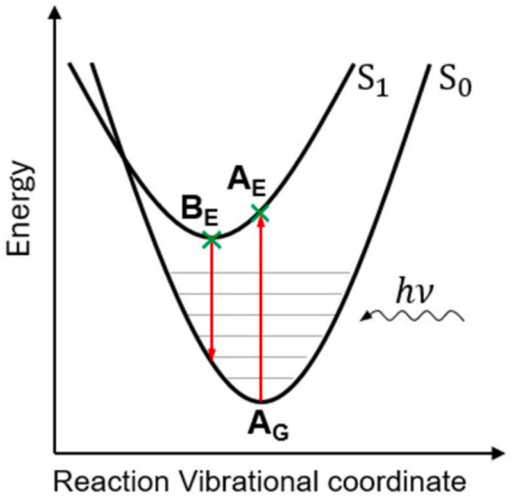

Fig. 5. Potential energy diagram of the ground and excited states of the D:A complex. $A_G \rightarrow A_E$ is the donor or acceptor of LE. B_E is the relaxed electron-hole polar on paired CT state. Reprinted from [13]. Copyrights 2023 AIP Publishing.

exciton dynamics in large systems with reasonable computational costs [15]. The method uses an approximate quantum chemical calculation technique (density functional tight binding (DFTB)) and exploits spatial locality in the DFTB formulation to treat spatially large systems without an explosive increase in the computational cost with the system size. In addition, efforts have been made to incorporate the effect of spin-orbit coupling [16]. Using this NA-MD method, the charge separation process at the interface between P3HT and [6,6]-phenyl-C_{61}-butyric acid methyl ester ($PC_{61}BM$) was successfully visualized and detailed analyses were performed, focusing on the effect of structural disorder at the interface (Fig. 7) [17]. First, the atomistic structure of the disordered P3HT(crystal):$PC_{61}BM$(amorphous) interface (Fig. 7a) was constructed via MD calculations using the NPT ensemble (GROMACS/GAFF). Subsequently, a local structural model (Fig. 7b) was extracted from the obtained interface structure and used in the following NA-MD simulations. At the beginning of the NA-MD simulation, the system was electronically excited by applying an oscillating electric field mimicking a light pulse (Fig. 7c), whose frequency was resonant with the excitation of P3HT (Fig. 7d). The time trace of the hole/electron densities is shown in Fig. 8, which provides an intuitive picture of exciton dynamics. At 100 fs, the entire P3HT region was positively charged (yellow) and a part of the $PC_{61}BM$ region was negatively charged (blue), indicating charge separation. After hundreds of femtoseconds (e.g., 500 fs), the negative charge diffused over the entire $PC_{61}BM$ region. The quantitative time traces of P3HT and $PC_{61}BM$ partial charges were obtained from the simulations. The simulations with considering the effect of the nuclear motion, suggested the progress of the charge separation within $\sim 10^2$ fs (Fig. 9a). When the effect of the nuclear motion was neglected (Fig. 9b), no significant charge separation was observed. These results indicate that nuclear motion plays a key role in charge separation in this system. The analyses in ref. [17] indicated that nuclear motion modulates the LUMO energy levels of P3HT to coincide with those of the neighboring acceptor molecules, thus facilitating electron transfer from the excited P3HT to $PC_{61}BM$. This method has broad potential applications in

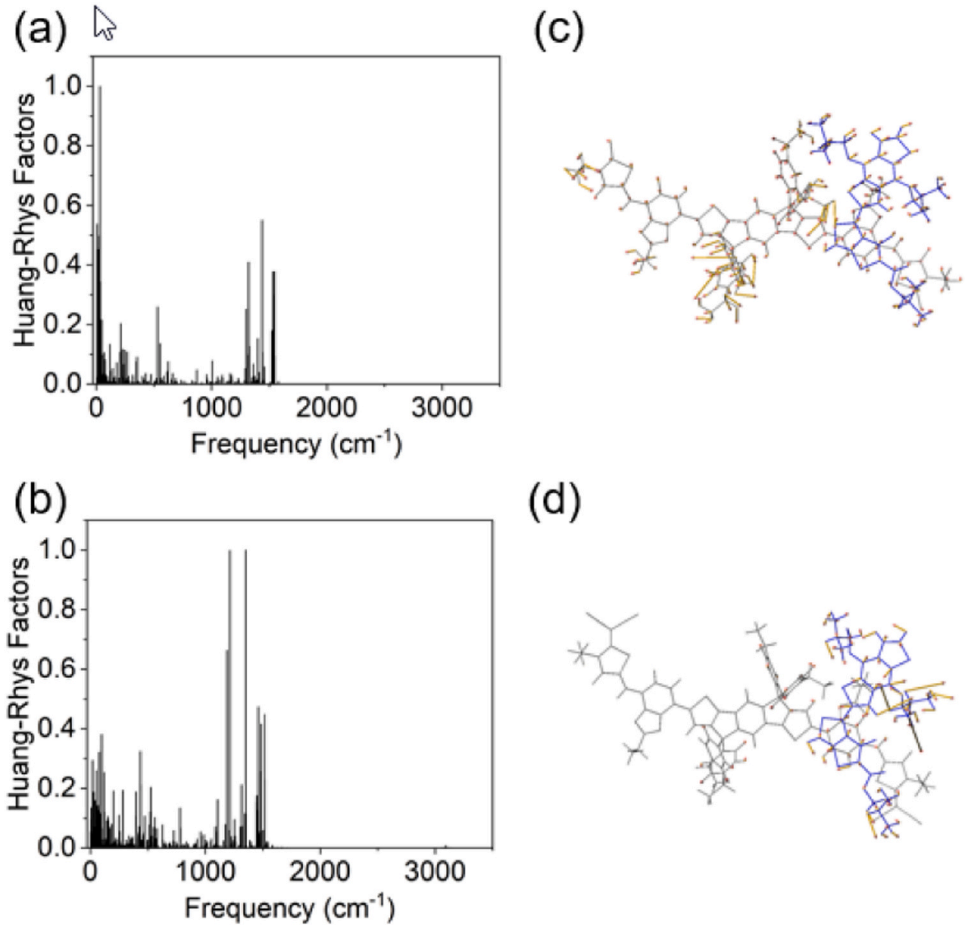

Fig. 6. The HR factor and with $B_E \rightarrow S_0$ process in (a) PTB7:BTA1 and (b) PTB7:BTA3, and normal mode vibration with $B_E \rightarrow S_0$ process in (c) 31 cm^{-1} in PTB7:BTA1 and (d) 1353 cm^{-1} in PTB7:BTA3. Adapted from [13]. Copyrights 2023 AIP Publishing.

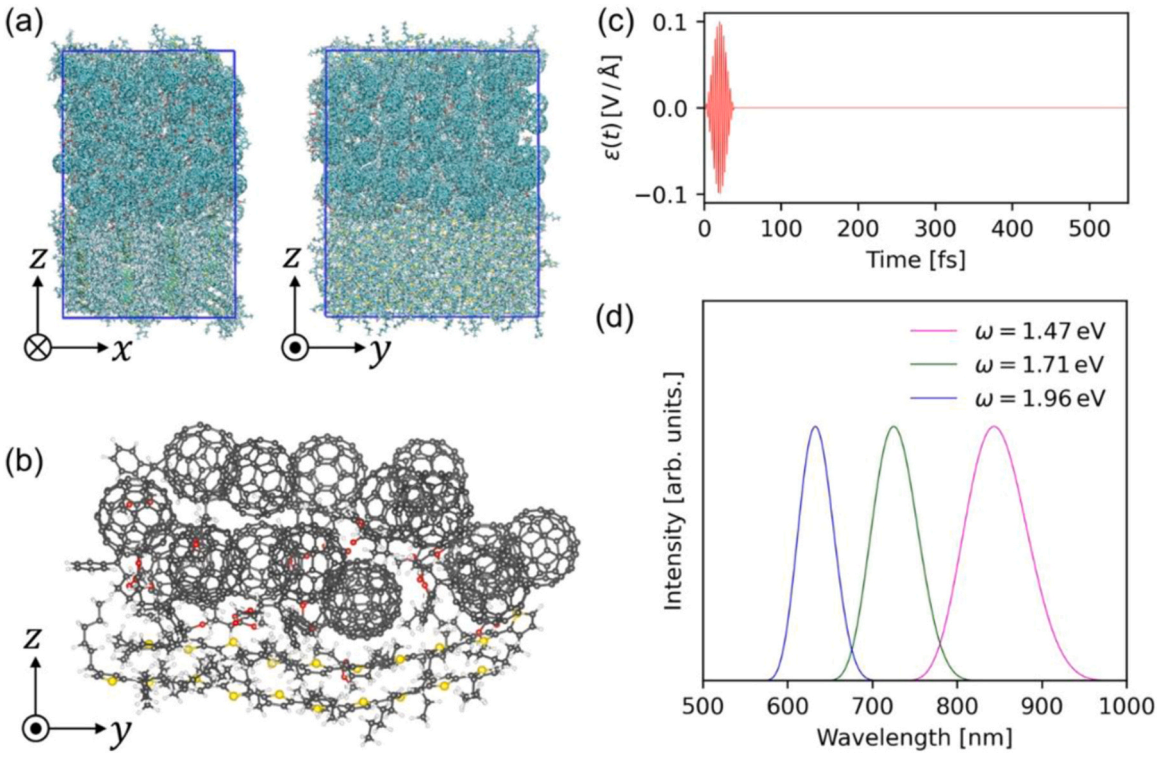

Fig. 7. (a) P3HT:$PC_{61}BM$ interface constructed using classical MD. (b) P3HT:$PC_{61}BM$ interface model used in the dynamics simulations, extracted from the MD-generated structure. The model consists of two P3HT molecules and 16 $PC_{61}BM$ molecules, totaling 1912 atoms. (c) Time-dependent evolution of electric field $\epsilon(t)$ for $\hbar\omega = 1.47$ eV. (d) Spectral densities of applied laser pulses for $\omega = 1.47$, 1.71, and 1.96 eV. Reprinted from Ref. [17]. Copyrights 2023 American Chemical Society.

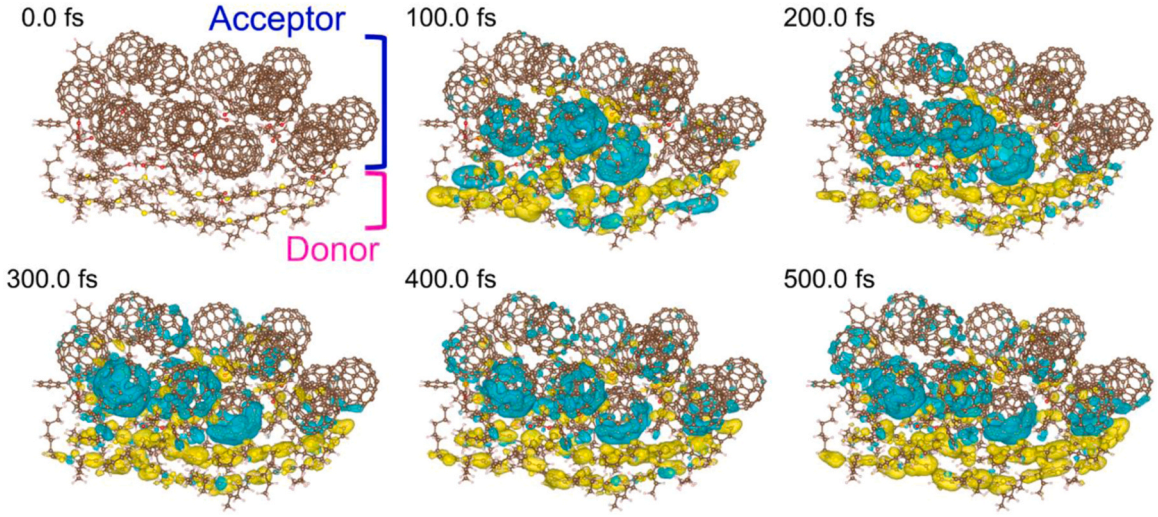

Fig. 8. Snapshots of the simulated hole (yellow) and electron (blue) densities.

photochemical phenomena such as photoinduced phase transitions [18].

3. Dye-sensitized solar cell

Two types of device architectures have been developed for organic solar cells: dye-sensitized solar cells (DSSC) and OPVs. In this review, thin-film OPVs will be focused on; however, before delivering the details of OPVs, an example of a DSSC related to dynamic excitons will be discussed. Higashino and Imahori et al. synthesized triarylamine (TAA)-appended gold(III) corrole dye TAA-AuCor (Fig. 10) [19]. DSSC with TAA-AuCor using the I_3^-/I^- redox shuttle exhibited a higher PCE than those with the reference dye AuCor without the TAA moiety. They clearly demonstrated that intramolecular electron transfer from the TAA moiety to the corrole radical cation can compete with charge recombination to realize a long-lived charge-separated state $TAA^{\bullet+}$-Cor/$TiO_2^{\bullet-}$. Consequently, the introduction of the TAA moiety effectively suppressed the undesirable charge recombination from an electron in the conduction band (CB) of TiO_2 to the dye radical cation and enhanced the PCE (Fig. 11).

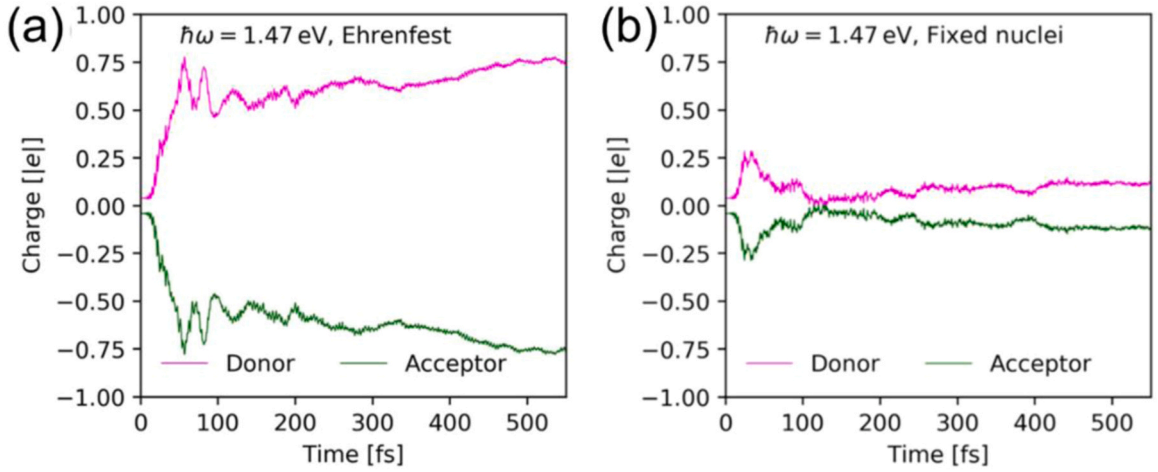

Fig. 9. Time-trace of the donor (P3HT) and acceptor ($PC_{61}BM$) Mulliken charges. (a) With including nuclear motion. (b) With nuclei fixed. Reprinted from Ref. [17]. Copyrights 2023 American Chemical Society.

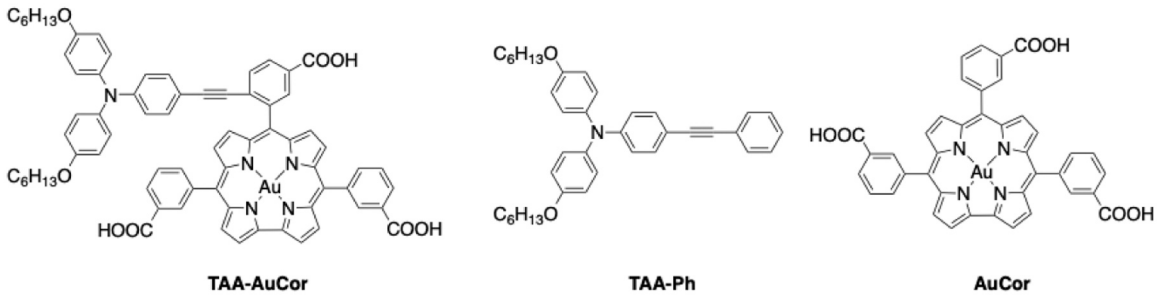

Fig. 10. Chemical structures.

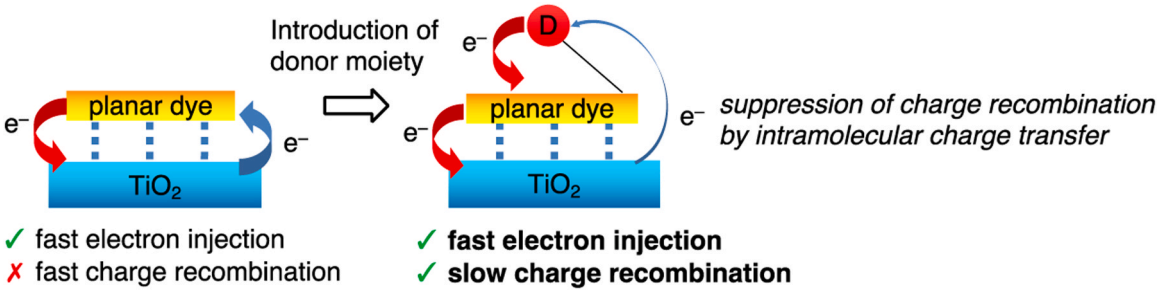

Fig. 11. Schematic representation of electron transfer processes for flat planar dyes with multiple anchoring groups. Intramolecular electron transfer from the donor moiety to the oxidized dye can inhibit undesirable charge recombination to enhance PCE. Adapted from Ref. [19]. Copyrights 2024 Wiley-VCH.

4. Development of novel organic semiconductor materials for OPVs

A photon-to-electron conversion process in OPVs is relies on the synergetic interplay of multiple materials. Consequently, the design of OPV materials is multifaced, requiring careful balance of various factors influencing the overall photovoltaic process. In 2017, Suzuki, Nakayama, Yamada et al. reported a series of diketopyrrolopyrrole (DPP)-tetrabenzoporphyrin (BP) conjugates, designated as C*n*-DPP−BP ($n = 4, 6, 8$, or 10, depending on the alkyl chain length on the DPP unit), as donor materials in BHJ OPVs, using $PC_{61}BM$ as the acceptor (Fig. 12) [20]. A comparative study revealed that the PCE of these systems was strongly influenced by the alkyl chain length of the DPP moiety. As the chain length increased, J_{SC} decreased from 15.2 ($n = 4$) to 0.88 mA cm^{-2} ($n = 10$), while PCE dropped from 5.2 % to 0.19 % (Fig. 13). Two-dimensional grazing incidence wide-angle X-ray diffractometry (2D-GIWAXD) indicated that the C4-DPP-BP molecule predominantly adopts a face-on geometry on the substrate, as illustrated in Fig. 14 [20,21]. Notably, the bottom section of Fig. 14 provides a schematic representation of the local aggregate structures. Atomic force microscopy further confirmed that the aggregates had a grain size of approximately 100 nm or smaller, facilitating efficient exciton migration and charge transport. In contrast, incorporating an n-decyl (C10) group into the DPP unit led to an edge-on molecular orientation and the formation of micrometer-sized aggregates. Remarkably, the molecular orientation in Cn-DPP–BP neat films exhibited a drastic change only by altering the alkyl-chain length. A possible explanation for this phenomenon is the molecular aspect ratio, as suggested by Chen et al.[22,23] and Bazan et al. [24,25]

The small molecular BHJ OPVs were suitable to study the dynamic exciton mechanism of OPVs in detail. Ohta et al. used time-resolved THz spectroscopy to investigate the charge-carrier dynamics of C4-DPP-BP:

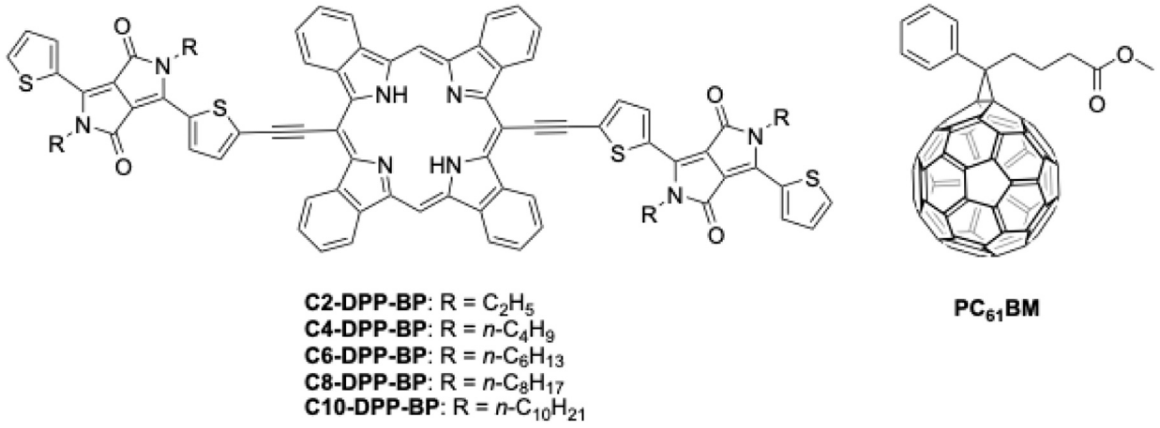

Fig. 12. Chemical structure of C*n*-DPP–BPs and $PC_{61}BM$.

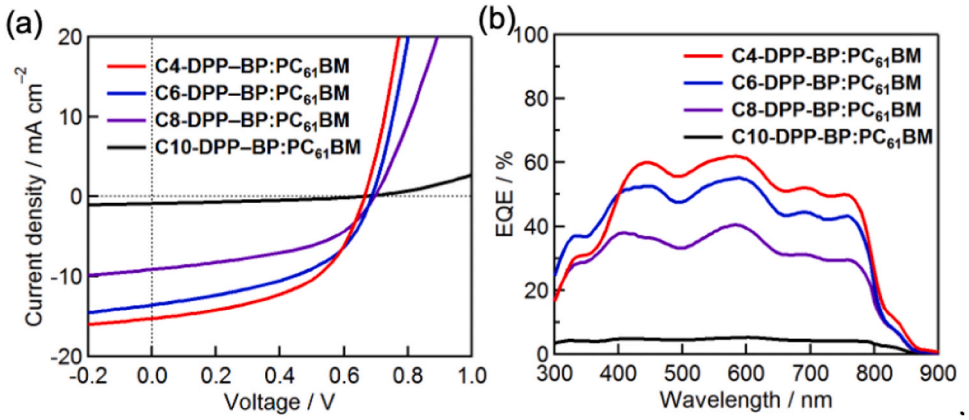

Fig. 13. (a) *J*–*V* curves and (b) EQE spectra of the best-performing BHJ cells. Measurements were conducted under AM1.5 G illumination at 100 mW cm^{-2}. Reprinted from [20]. Copyrights 2017 The Royal Chemical Society.

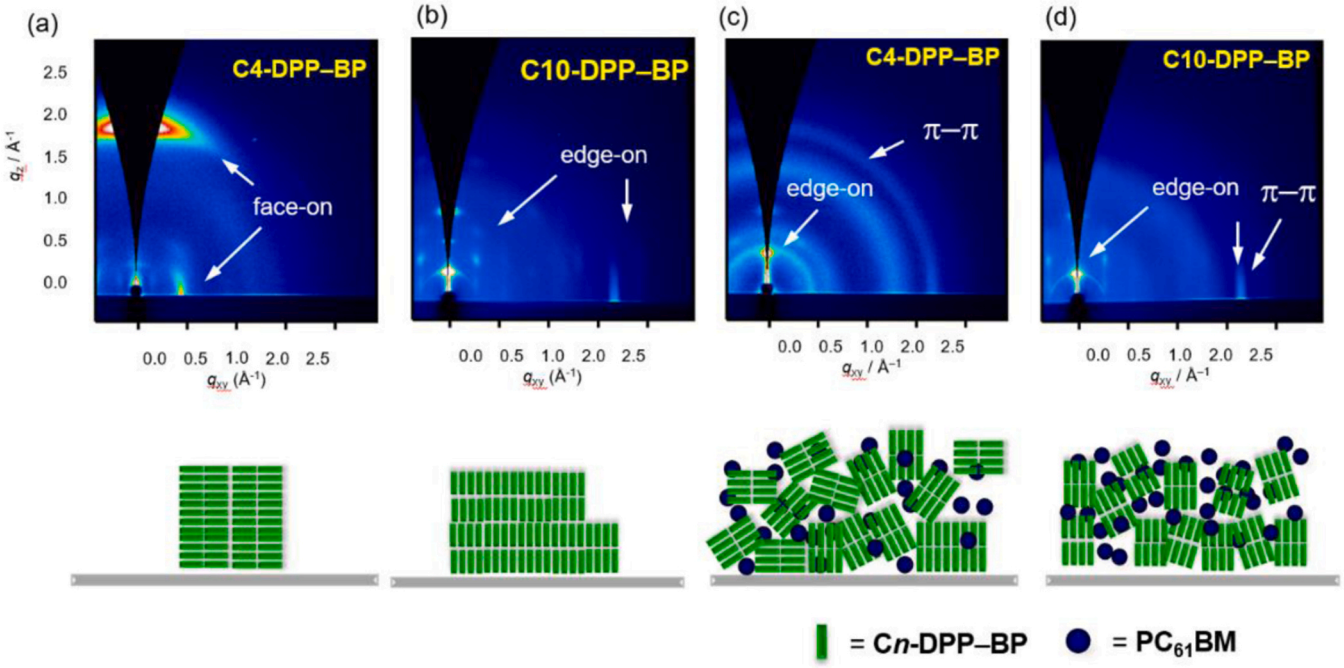

Fig. 14. 2D-GIWAXD images (top) and schematic aggregation orientation illustration (bottom) of (a) C4-DPP-BP, (b) C10-DPP-BP, (c) C4-DPP-BP:$PC_{61}BM$, and (d) C10-DPP-BP:$PC_{61}BM$ films. Reprinted from [21]. Copyrights 2022, American Chemical Society.

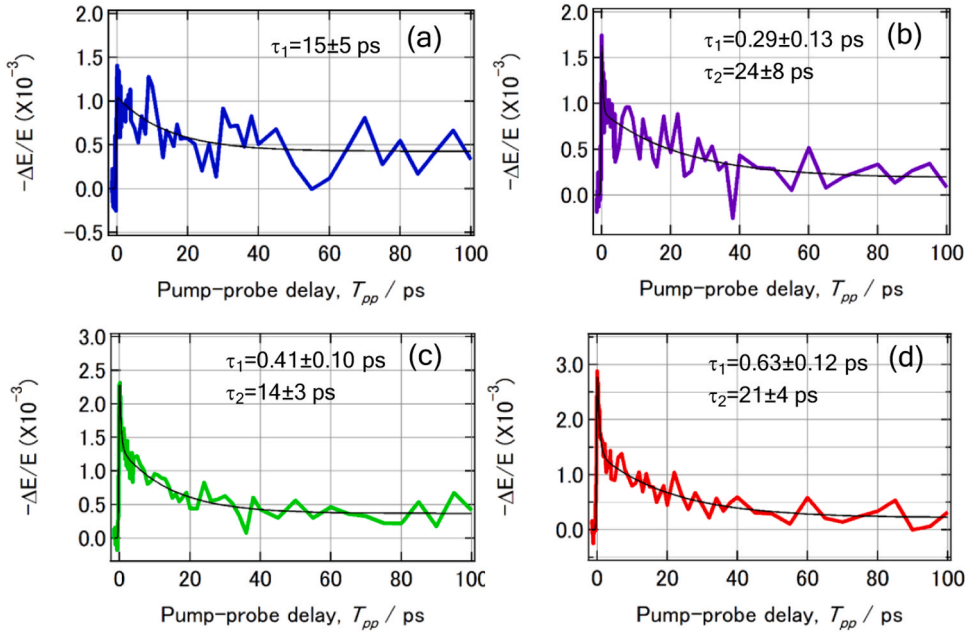

Fig. 15. Photoinduced changes in the THz electric fields in C4-DPP-BP:$PC_{61}BM$ BHJ films. Escitation wavelength: λ_{EX} = 800 nm. Thick solid lines represent experimental data, while black lines indicate double-exponential fits obtained via convolution with the instrument response function. Excitation fluences were (a) 140 μJ/cm^2, (b) 230 μJ/cm^2, (c) 300 μJ/cm^2, and (d) 540 μJ/cm^2. Reprinted from [27]. Copyrights 2020 Elsevier.

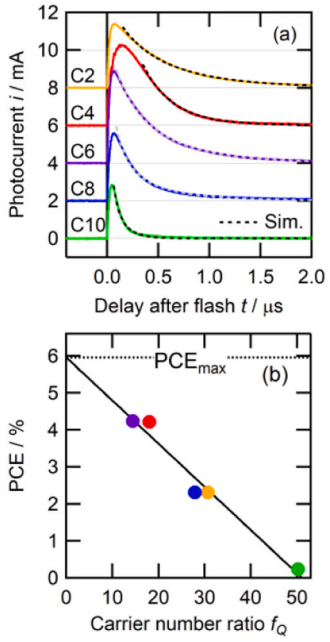

Fig. 16. (a) Time-resolved transient photocurrent profiles of C*n*-DPP-BP:$PC_{61}BM$ BHJ devices under short-circuit conditions, measured using nanosecond pulse excitation (λ_{EX} = 532 nm) with a fluence of 63 μJ/ cm^2. (b) Correlation between PCE and the ratio of recombined carriers to extracted carriers under short-circuit conditions. Reprinted from [21]. Copyrights 2022 American Chemical Society.

$PC_{61}BM$ BHJ thin films [26–28]. For an excitation fluence of 540 μJ/cm^2, the decay time constants of the time-resolved THz signals are 0.5 and 14 ps, which result from the relaxation of the bound polaron pair (Fig. 15). The amplitude of the sub-picosecond decay in the time-resolved THz signal is sensitive to the fluence of the optical excitation pulse and this decaying component at a higher fluence was considered to originate from polaron pair annihilation. They also compared the charge-carrier dynamics of C10-DPP-BP:$PC_{61}BM$ and C4-DPP-BP:$PC_{61}BM$ based BHJ films [28]. In contrast to the difference in PCE mentioned above, the product of carrier mobility and the yield of the photogenerated charge carriers are similar to each other. This similarity can be attributed to the distinct properties of the local mobility at a 10 nm length-scale probed by time-resolved THz spectroscopy, which is different from the long-range transport of the charge carriers.

Ikoma et al. performed sub-microsecond time-resolved photocurrent measurements using a nanosecond pulse laser to investigate charge carrier recombination in the active layer of C*n*-DPP- BP:$PC_{61}BM$ BHJ OPVs (n = 2, 4, 6, 8, 10), [21,29]. The photocurrent decay profile increasingly deviated from an exponential trend as the alkyl chain length (n) increased (Fig. 16a). Macroscopic charge mobility is governed by carrier hopping between multiple crystalline domains, as shown in Fig. 14. In this structure, the p:n interface likely exhibits a large surface area oriented normal to the internal electric field, promoting efficient non-geminate recombination. This recombination mechanism significantly influences the J_{SC}, which is a key determinant of the overall PCE in these devices. Fig. 16b shows the relationship between PCE and the ratio (f_Q) of the number of recombined carriers (Q_{re}) to extracted carriers (Q_{ex}) under short-circuit conditions. This straightforward analysis suggests that minimizing non-geminate recombination—by spatially separating the carrier transport layers from the carrier generation layer—could enhance the PCE of Cn-DPP-BP:$PC_{61}BM$ BHJ OPVs, potentially reaching up to 6 %.

Kobori et al. elucidated the microscopic origins of photocarrier generation, revealing that phonon-assisted one-dimensional (1D) electron–hole dissociations at the D:A interface plays a crucial role. Their study focused on C4-DPP−H_2BP and its zinc complex, C_4-DPP−ZnBP, as small-molecule donors in combination with $PC_{61}BM$ [30]. Using time-resolved electron paramagnetic resonance (EPR), they characterized controlled charge recombination by modulating disorder in the π−π donor stacking (Fig. 17). This stacking arrangement facilitates carrier transport by stabilizing molecular conformations, thereby suppressing nonradiative voltage loss and selectively capturing interfacial radical pairs separated by 1.8 nm in bulk-heterojunction OPVs. Fig. 17d shows a geometric model of the separated geminate radical pair (RP) at N = 5, which induces selective triplet recombination through a gate effect

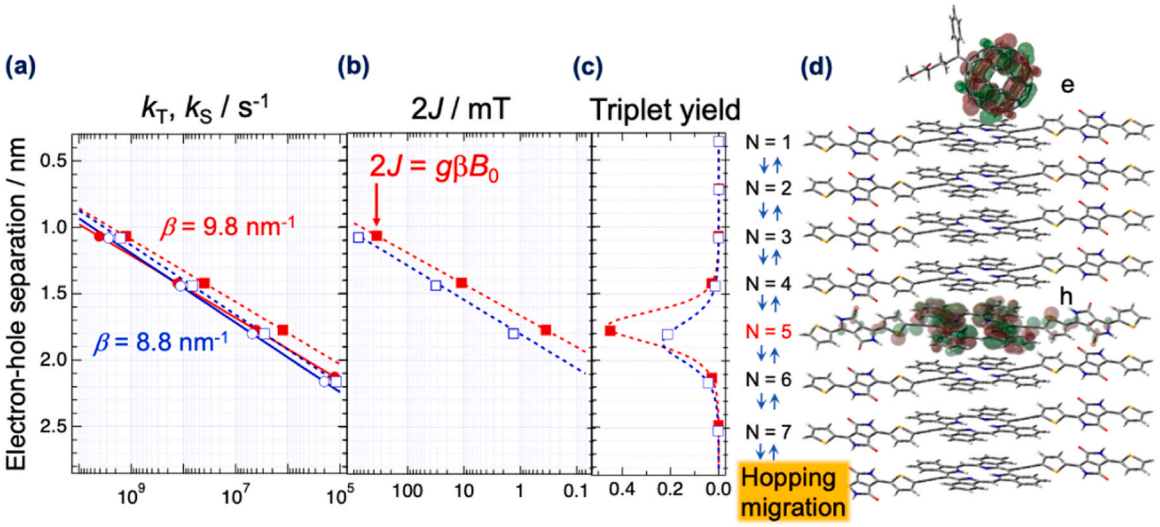

Fig. 17. (a) Charge recombination rate constants of $k_T(r)$ (solid lines and circles) and $k_S(r)$ (dashed lines and squares). β: the attenuation factor in the r dependence of the electronic coupling. (b) $|S\rangle$ -$|0\rangle$ electronic energy gap (2 J). (c) Quantum yields of the triplet exciton products via $|S\rangle$ -$|0\rangle$ conversion as a function of the separation distance. C4-DPP-$H_2BP^{+\bullet}$:$PC_{61}BM^{-\bullet}$ (red) and of C4-DPP-$ZnBP^{+\bullet}$:$PC_{61}BM^{-\bullet}$ (blue) at $t = 0.5$ μs. (d) Corresponding geometry model of the separated geminate RP at $N = 5$. Reprinted from [30]. Copyright © 2022 The Authors. Published by American Chemical Society. This publication is licensed under CC-BY-NC-ND 4.0.

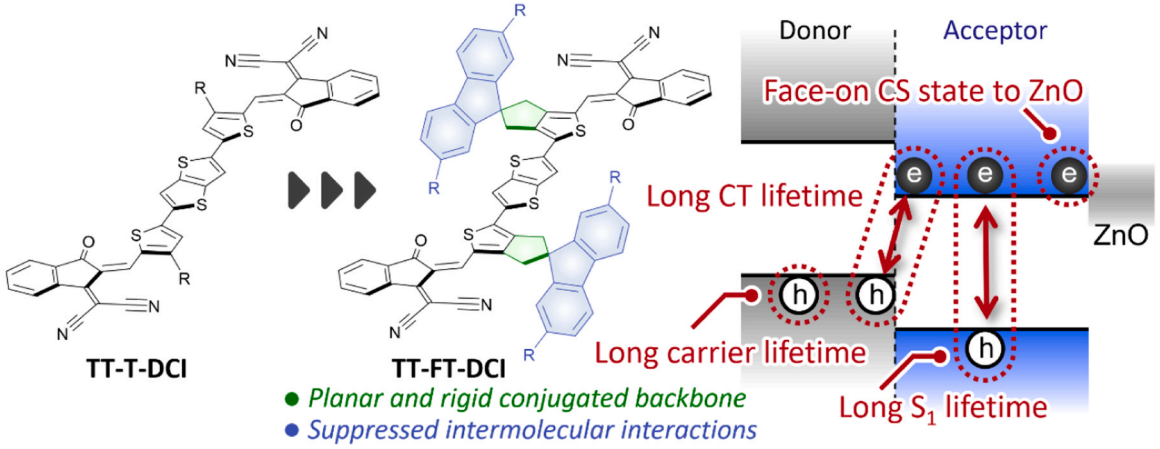

Fig. 18. Chemical structures of TT-T-DCI and TT-FT-DCI and structure-OPV mechanism relationship in this study. Adapted from [39]. Copyrights 2022 The Royal Society of Chemistry.

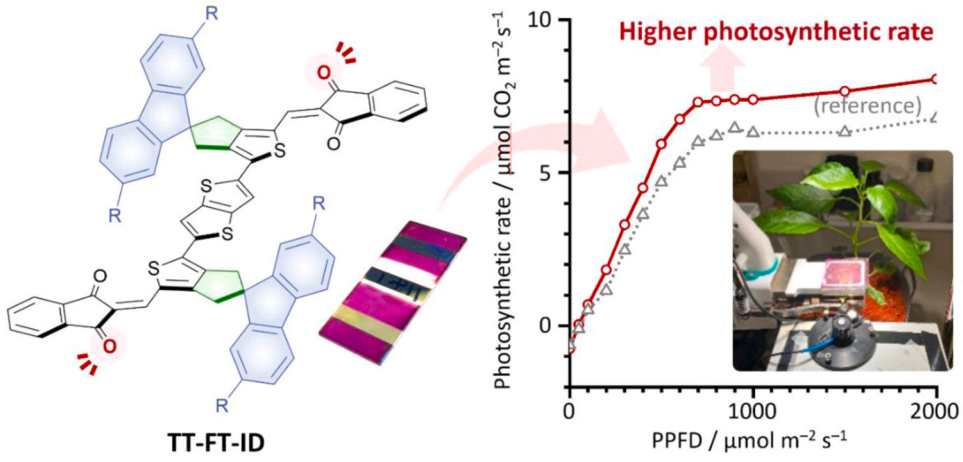

Fig. 19. Chemical structure of TT-FT-ID and photosynthetic rate measurements using TT-FT-ID. PPFD indicates photosynthetic photon flux density. Adapted from [40]. Copyrights 2024 The Royal Society of Chemistry.

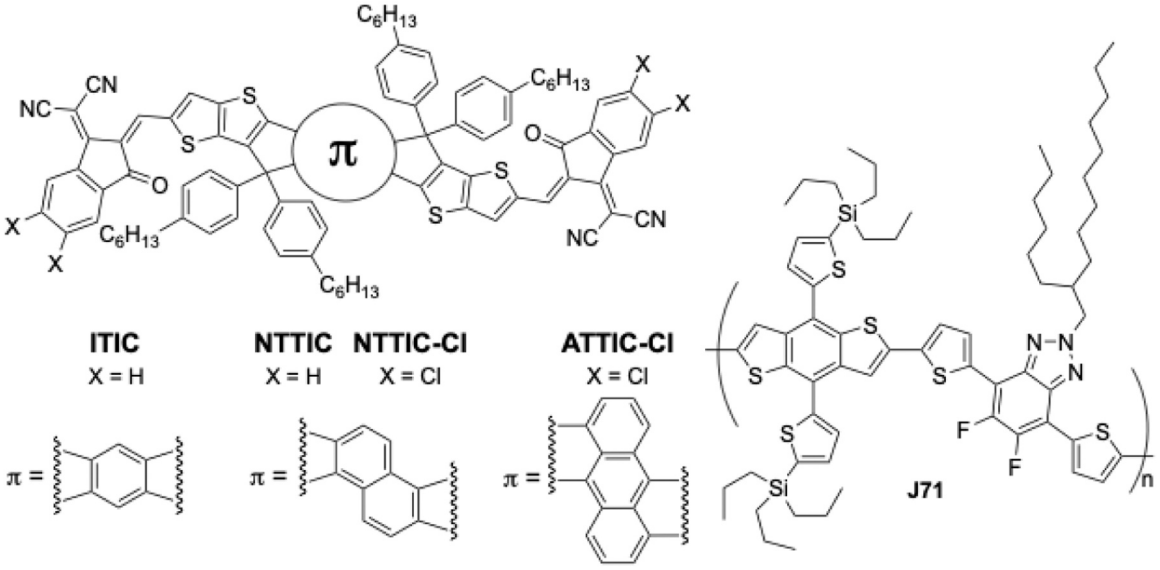

Fig. 20. Chemical strictures of ITIC, NTTIC, NTTIC-Cl, ATTIC-Cl, and J71.

during hole migration. their findings indicate that a high degree of crystalline order enhances backscattering phonon interactions, leading to increased geminate charge recombination and, consequently, a reduction in V_{oc}.

Non-fused electron-accepting π-conjugated compounds have also been explored for use in NFAs in OPVs [31–36], but the effect of flexible non-fused structures on electron-hole dynamics is not well understood. Ie et al. showed that the incorporation of cyclopentene annelation into the thiophene moiety is an effective approach to improve the planarity and rigidity of π-conjugation in repeated oligothiophenes (Fig. 18) [37, 38]. Thus, Ie et al. developed a non-fused NFA (TT-FT-DCI) using a rigid bulky FT unit (Fig. 18) [39]. OPVs with TT-FT-DCI and the donor polymer PBDB-T achieved a PCE of 6.19 %, owing to the increased *J*sc and fill factor compared to those of TT-T-DCI. Time-resolved IR absorption spectroscopy showed that TT-FT-DCI undergoes less conformational relaxation than TT-T-DCI under photoexcitation owing to its rigid π-conjugated framework. TT-FT-DCI also exhibited longer lifetimes for the excited and CS states in blend films. Flash-photolysis time--resolved microwave conductivity (FP-TRMC) measurements indicated a longer free carrier lifetime in PBDB-T, and time-resolved electron paramagnetic resonance (TREPR) measurements revealed a face-on conformation near the ZnO electrode, which was attributed to the suppression of aggregation by the bulky spiro-fluorene moiety. This study highlights the advantages of rigid, bulky, non-fused NFAs in improving photon-to-current conversion in OPVs.

The rigidity of the π-conjugated skeleton and suppression of H-aggregation through the introduction of FT units were found to effectively reduce the full width at half maximum (FWHM) of the absorption spectrum of the films. Consequently, Ie et al. designed a new acceptor, TT-FT-ID, with absorption in the green light wavelength region by modifying the electron-withdrawing terminal units from dicyanomethylidene indanone (DCI) to 1,3-indanone (ID) (Fig. 19) [40]. By combining TT-FT-ID with the donor polymer P3HT, which also absorbs green light, the resulting OPVs were found to be suitable for agrivoltaics, selectively utilizing green light wavelengths to generate electricity.

A systematic investigation into the relationship between the molecular structure and photovoltaic performance of acceptor–donor–acceptor (A–D–A)-type NFAs is crucial for establishing design guidelines for high-performance OPVs. To explore the impact of π-conjugation size in the central D core of A−D− A-type NFAs, Imahori et al. developed NTTIC, where the central benzene of the benchmark NFA, ITIC, was replaced with naphthalene (Fig. 20) [41]. The NTTIC film showed a slightly smaller optical gap, higher LUMO energy level, and enhanced π–π stacking compared to ITIC. Notably, the singlet exciton lifetime of the NTTIC film (180 ps) was longer than that of the ITIC film (140 ps) due to the stronger intermolecular interaction in the NTTIC film. In combination with a typical donor polymer PBDB-T, the NTTIC-based OPV device achieved a higher PCE (9.95 %) than the ITIC-based device (9.71 %). Despite the larger domain size of NTTIC in the PBDB-T:NTTIC blend film compared with that of ITIC in PBDBT: ITIC, the exciton diffusion efficiency (ED) to the donor:NFA interface in PBDB-T:NTTIC was substantially high (>95 %) owing to the sufficiently long singlet exciton lifetime of NTTIC.

Additionally, naphthalene-cored NFA with chlorinated IC groups, NTTIC-Cl, were synthesized (Fig. 20) [42]. The NTTIC-Cl film showed broadened absorption, a downshifted LUMO energy level, and an elongated singlet exciton lifetime (250 ps) compared to those of the NTTIC film. When blended with the conjugated donor polymer J71, the NTTIC-Cl-based OPV device showed a higher J_{SC} (19.6 mA cm^{-2}) than the NTTIC-based device (15.6 mA cm^{-2}). As a result, the J71: NTTIC-Cl-based device was superior (10.5 %) to the J71:NTTIC-based device (PCE = 9.25 %).

Imahori et al. also developed an anthracene-cored NFA with chlorinated IC groups (ATTIC-Cl, Fig. 20) [43]. In contrast to ITIC and NTTIC, which feature highly planar backbones, ATTIC-Cl adopts a non-planar structure because of the lack of coplanarity between the anthracene and thieno[3,2-*b*]thiophene units. Despite the longer singlet exciton lifetime of the ATTIC-Cl film (570 ps), the J71:ATTIC-Cl-based device exhibited a PCE 7.1 % lower than that of the J71:NTTIC-Cl-based device, which is attributed to the inferior electron-transporting properties of ATTIC-Cl. These studies collectively demonstrate that subtle modifications in the central core structure, such as replacing benzene with naphthalene or anthracene, can significantly influence the exciton dynamics and photovoltaic properties of A–D–A type NFAs.

Photon-to-current conversion in OPVs involves a multistep process in which a photon generates an exciton in the donor or acceptor, followed by the separation of an exciton into a free electron and a hole. The energy required to separate the exciton beyond the Coulomb force of attraction is called the exciton binding energy (E_b) and is classically expressed by Eq. (1):

$$E_b \approx \frac{e^2}{4\pi\varepsilon_0\varepsilon_r \quad R} \tag{1}$$

where e is the elementary charge, ε_0 is the vacuum dielectric constant, ε_r

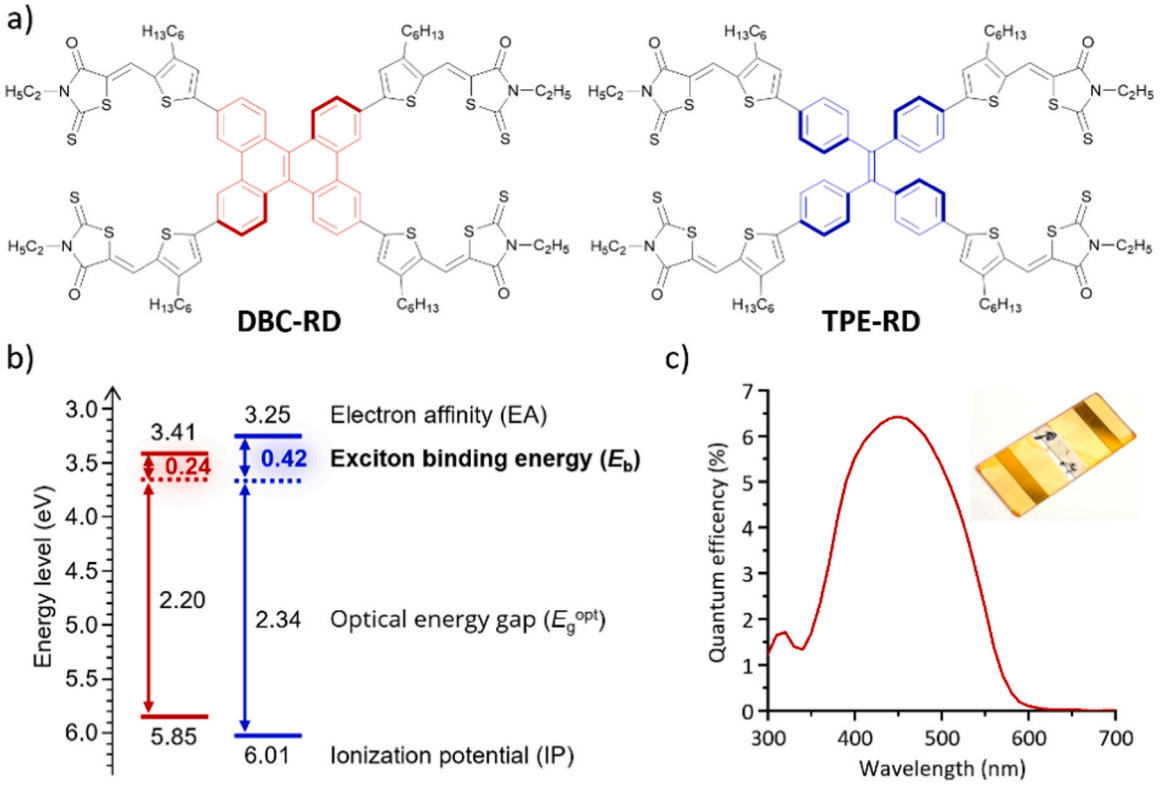

Fig. 21. (a) Chemical structures and (b) energy diagram of DBC-RD, TPE-RD, and (c) EQE spectrum of DBC-RD-based single-component OPVs. Adapted from [51]. Copyrights 2024 Wiley-VCH.

is the dielectric constant of the molecule, and R is the average electron–hole distance in the molecule. Organic semiconductor materials typically have E_b values in the range of 0.3–0.6 eV, which are significantly larger than the thermal energy at room temperature. This large E_b is considered to be a major factor contributing to energy loss and charge recombination in OPVs. Therefore, the establishment of a molecular design that can achieve lower E_b in the solid state has become a crucial objective in the pursuit of high-performance OPVs. Recent experimental studies suggest that strategies such as the extension of π-conjugated skeletons and the introduction of polar functional groups are part of an effective molecular design to reduce E_b by modulating the dielectric properties at the single-molecule level [44–48].

Theoretical studies indicate that the assembled structures in the solid state have a significant impact on the E_b of organic semiconductors, with aggregation and dimensional packing playing a crucial role in enhancing the electronic polarization [45,49,50]. However, experimental studies exploring the direct relationship between molecular aggregation and E_b remain limited. Ie et al. investigated the effects of molecular aggregation on E_b and carrier generation efficiency by comparing two semiconducting materials, DBC-RD and TPE-RD, based on the central unit of dibenzo[*g*,*p*]chrysene (DBC) and tetraphenylethylene (TPE), which exhibit different aggregation behaviors: π-π stacking for DBC and T-shaped stacking for TPE (Fig. 21) [51]. While these molecules exhibited similar single-molecule properties, DBC-RD showed a smaller E_b (0.24 eV) and larger dielectric constants in the pristine films, attributed to intermolecular interactions. In contrast, the matrix-diluted films of both compounds showed similar E_b values, further supporting the role of molecular packing in modulating E_b. In single-component OPVs, DBC-RD exhibited a photovoltaic response with an EQE of 6.4 %, whereas TPE-RD showed no such characteristics. Additionally, DBC-RD

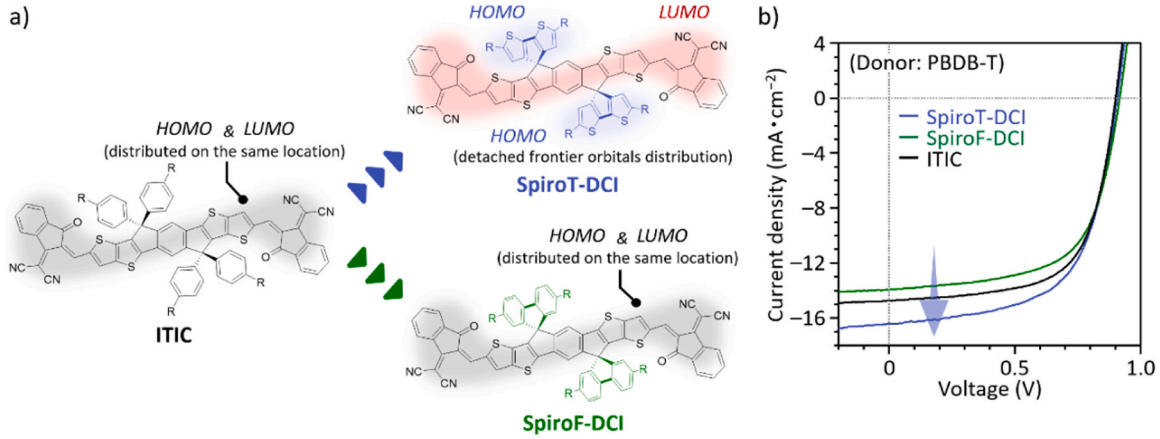

Fig. 22. Chemical strictures of ITIC, SpiroT-DCI, and SpiroF-DCI, and *J*-*V* curves based on these acceptors. Adapted from [52]. Copyrights 2024 Wiley-VCH.

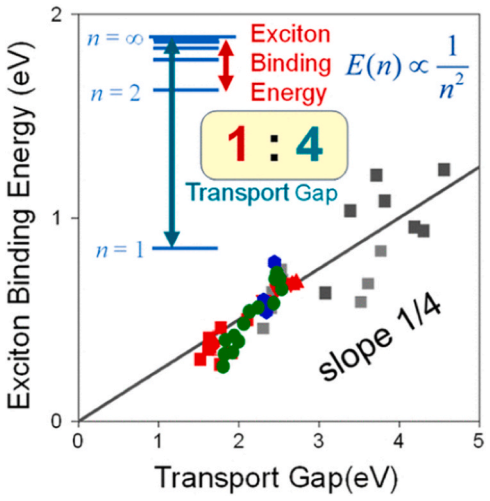

Fig. 23. Relationship between the exciton binding energies and the bandgaps (transport gaps) for 42 organic solar cell materials (15 NFAs (red), 4 fullerene acceptors (blue), 13 low-bandgap polymers (green), 7 organic light-emitting diode materials (black), and 3 crystalline materials (gray)). Reprinted from [53]. Copyright © 2023 The Authors. Published by American Chemical Society. This publication is licensed under CC-BY-NC-ND 4.0.

demonstrated superior photocatalytic activity in a heterogeneous OPC reaction compared with TPE-RD. These findings highlight the critical influence of molecular aggregation on the E_b and device performance.

According to Eq. (1), increasing the electron–hole separation (R) in the photoexcited state is expected to lower the E_b of organic semiconductors. Ie et al. demonstrated that introducing spiro-substituted biphenyl units can enhance the performance of non-fused NFA TT-FT-DCI by modulating the frontier molecular orbital (FMO) energy levels [39]. The π-extended biphenyl unit modulates the FMO energy levels by altering its chemical structure. The HOMO energy level of the fluorene unit was slightly higher than that of the commonly used acceptor ITIC. By replacing the biphenyl unit with an electron-donating bithiophene unit, the shallow HOMO energy level could be adjusted, resulting in a shift in the electronic distribution of the HOMO from the conjugated backbone of ITIC to the bithiophene unit. This modification provides a strategic approach to tuning the FMO distribution in organic semiconductors. Therefore, Ie et al. designed two ITIC-based NFAs, SpiroT-DCI and SpiroF-DCI, with spiro-substituted bithiophene and biphenyl units, respectively, to fine-tune the FMO distributions (Fig. 22) [52]. The HOMO of SpiroT-DCI was localized on the bithiophene unit, leading to a smaller E_b (0.32 eV) than that of SpiroF-DCI (0.40 eV) and ITIC (0.41 eV). This reduction in E_b was attributed to the separated FMO distribution in SpiroT-DCI, resulting in a significantly improved performance in single-component OPVs based on this material. Moreover,

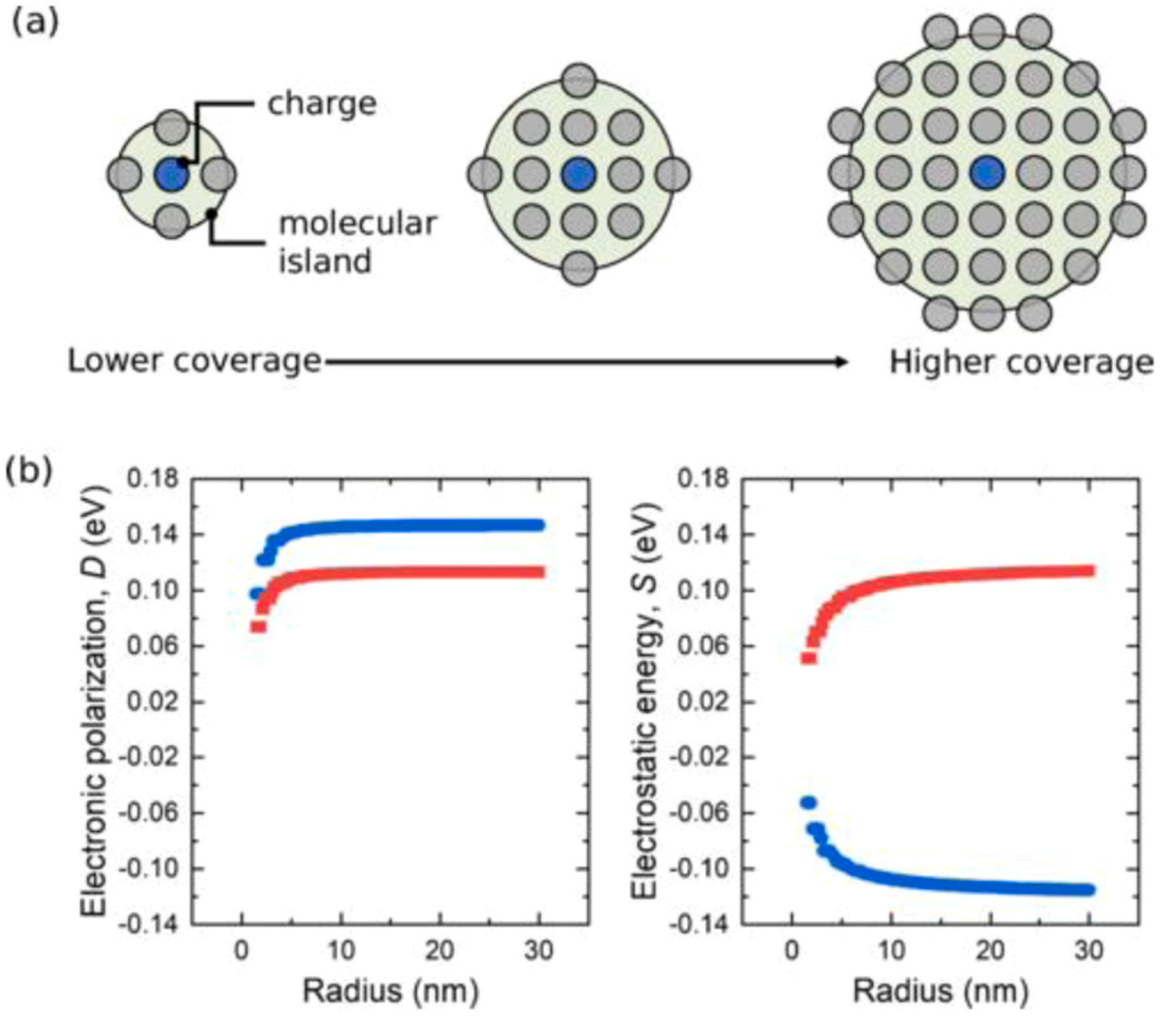

Fig. 24. (a) The disk model for the growing island without a changing lattice constant. (b) The calculated point charge-induced dipole interaction (D) and the point charge-permanent quadrupole interaction (S). The calculations for ZnPc and F16 × ZnPc are indicated by blue circles and red squares. Reprinted from [54]. Copyrights 2022 American Physical Society.

BHJ OPVs using PBDB-T and SpiroT-DCI achieved a maximum PCE of 9.08 %, which was higher than that of OPVs based on SpiroF-DCI (8.04 %) and ITIC (8.62 %). Time-resolved infrared absorption spectroscopy and photoluminescence decay studies revealed more efficient charge separation and longer free carrier lifetimes for SpiroT-DCI than for SpiroF-DCI and ITIC. These findings suggest that tuning the FMOs to increase electron–hole separation is a promising strategy for reducing E_b and enhancing OPV performance.

5. Evaluation of OPV devices

Yoshida et al. developed a novel technique called low-energy inverse photoelectron spectroscopy (LEIPS) to study the unoccupied states of organic semiconductors, polymers, and perovskite materials. LEIPS allows the precise determination of electron affinities, giving us access to previously unattainable energy parameters such as E_b, polarization energy, and electrostatic energy. The E_b values of organic semiconductors and polymers are large and much larger than the thermal energy. Therefore, excitons in these materials cannot dissociate spontaneously, which is crucial for the operation of organic optoelectronic devices. However, accurate experimental data on the exciton binding energies of organic semiconductors are lacking. Yoshida et al. determined E_b as the difference between the optical and transport bandgaps, with a precision of 0.1 eV. In particular, the electron affinities determined by LEIPS with a precision better than 0.05 eV allow us to determine the transport gap and exciton binding energies with such high precision. Through a systematic comparison of a wide range of organic semiconductors, including 42 organic solar cell materials (15 NFAs, 4 fullerene acceptors, 13 low bandgap polymers, 7 organic light emitting diode materials, and 3 crystalline materials), it was found that the exciton binding energy is a quarter of the transport gap, regardless of the material (Fig. 23). This unexpected relationship was interpreted from a hydrogen atom-like model, i. e. the quantized energy levels in a Coulomb potential between the positive and negative charges. This relationship between the exciton binding energy and the bandgap suggests that the optimal bandgap for the best power conversion efficiency of organic solar cells may be smaller than previously predicted [53].

The energy levels of an organic semiconductor are mainly determined by the molecular orbital energies of the constituent molecules. However, owing to the long-range nature of the Coulomb interaction, the electrostatic potential generated by the permanent molecular quadrupole moment can also affect the energy levels. Recent studies have shown that the energy levels can be changed by as much as 1 eV by the molecular orientation in the film or the molecular mixing ratio in the binary film due to intermolecular electrostatic interactions. Since theory predicts that the electrostatic energy should depend on the sample shape, we investigated the coverage-dependent energy levels of zinc phthalocyanine and perfluorinated zinc phthalocyanine in the submonolayer region using ultraviolet photoelectron spectroscopy (UPS) and LEIPS. From the coverage-dependent ionization energy and electron affinity, the electronic polarization energy and electrostatic energy were evaluated separately as a function of coverage. Unlike electronic polarization, which contributes only up to 10 meV, electrostatic energy contributes up to 120 meV to the coverage-dependent energy shift (Fig. 24) [54]. The coverage-dependent energy level shift is due to the sample shape-dependent energy level resulting from the long-range nature of the charge-permanent quadrupole interaction. The results suggest that the energy levels at the bulk heterojunction should vary depending on the interfacial structure and the molecular orientation at the D:A interface.

The charge carrier mobility is a crucial parameter in OPVs because it influences charge separation, recombination, and collection. High mobility, along with well-balanced hole and electron mobility, typically enhances charge transport by minimizing recombination losses, thereby improving the OPV performance [55,56]. Mobility is conventionally measured using direct current (DC) methods, which apply an electric field to an electrode-attached device and measure the current-voltage characteristics or transit time after photocarrier generation. Therefore, the resultant mobility is a time- and spatially averaged value across the transport distance. However, the mobility is likely time-dependent, relaxing from the high-energy state after photogeneration (Fig. 25a). This phenomenon falls under the concept of dynamic excitons, which focuses on the dynamic behavior of excitons and charge carriers [5]. The relaxation process occurs over distances ranging from nanometers to micrometers and timescales ranging from picoseconds to microseconds, aligning with typical OPV dimensions and transit times. Time-resolved measurements using alternating current (AC) electric fields including light, microwaves, and terahertz radiation are ideal for probing this relaxation process [57]. A physical aspect of this relaxation was illustrated by Melianas et al. (Fig. 25b), where a “hot” charge carriers relax into the density of state or are captured by traps, resulting in a decrease in mobility [58].

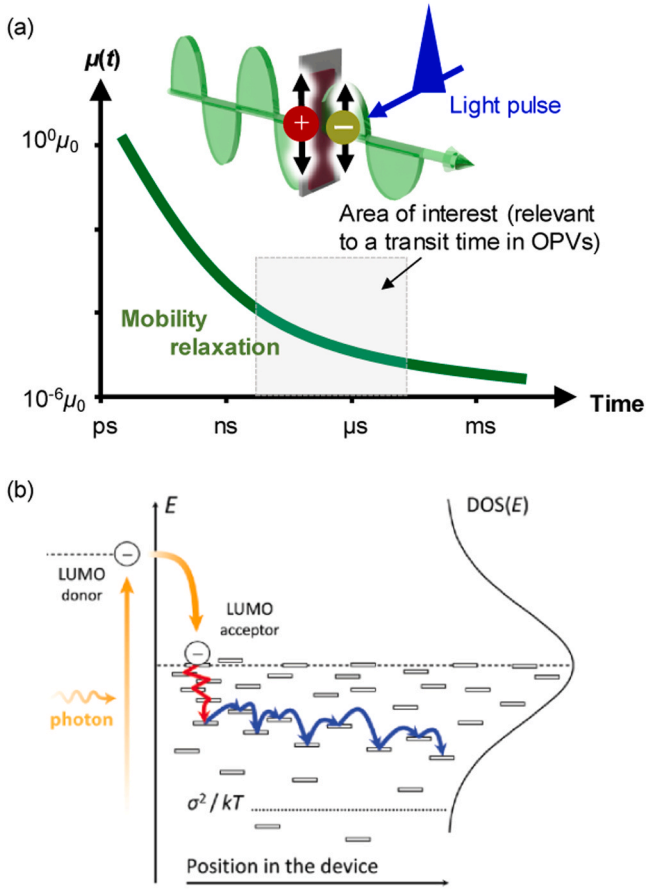

Fig. 25. (a) Schematic of relaxation of charge carrier mobility as a function of time. An illustration of electrode-less measurements (e.g. TRMC) is superimposed. (b) Charge carrier relaxation into DOS, reprinted from [58]. Copyrights 2019 Wiley-VCH.

Saeki et al. reported a combined method of time-of-flight (TOF) and TRMC that enables simultaneous measurements of TOF mobility (DC mobility) and TRMC photoconductivity (AC mobility) [59]. By comparing the results of three fullerene-based OPVs (P3HT:PCBM, PCPDTBT:PCBM, and PffBT4T:PCBM), the highly crystalline PffBT4T:PCBM films showed the slowest relaxation of hole mobility, followed by the crystalline P3HT:PCBM and less crystalline PCPDTBT:PCBM films. This order is consistent with the optimal thickness of the OPVs and reflects the relationship between the charge-carrier relaxation and device performance parameters. Furthermore, the measurements were applied to NFA-based OPVs (PBDB-T:ITIC or Y6, Fig. 26a), revealing that the relaxation of the hole and electron mobilities are correlated with the fill

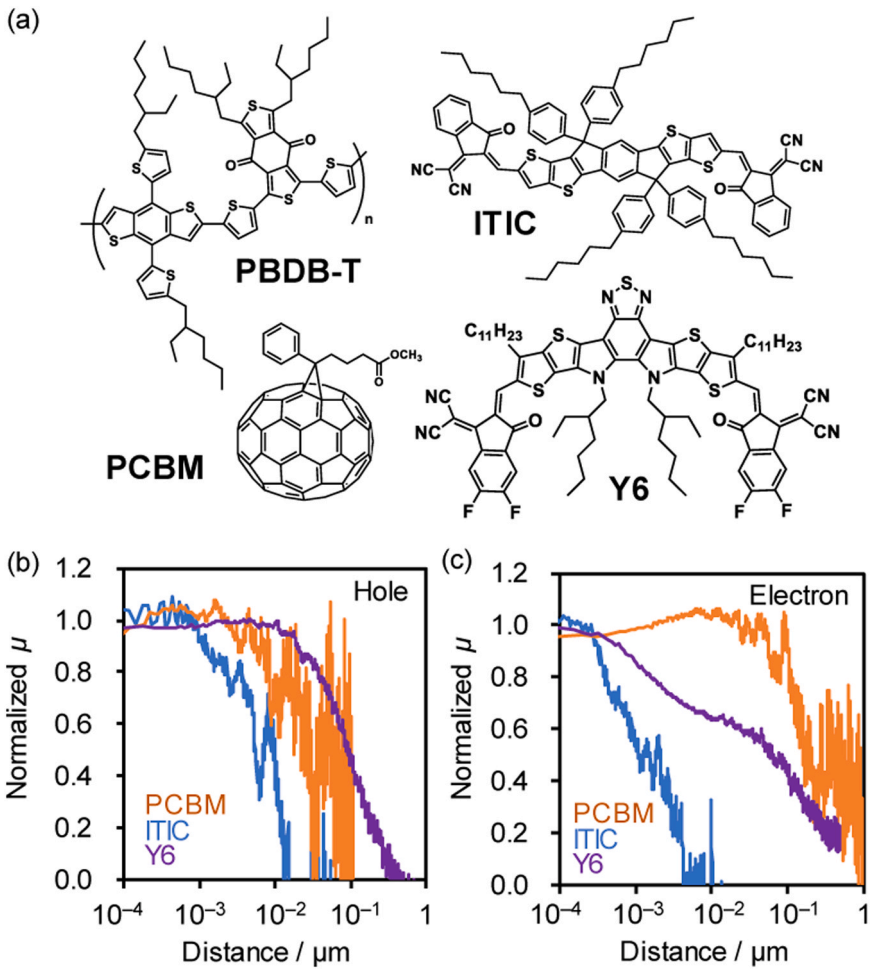

Fig. 26. (a) Chemical structure of PBDB-T, PCBM, ITIC, and Y6 used for the TOF-TRMC measurements. (b) Hole and (c) electron mobility relaxation as a function of distance (the vertical direction of an OPV device). Adapted from [60]. Copyrights 2021 Wiley-VCH.

factors (Figs. 26b and 26c)[60]. In particular, the highly crystalline Y6, which forms a 3-diemensional assembly [61], exhibits slow electron relaxation compared to ITIC. The measurements and analyses were extended to evaluate the optimal thickness of the OPVs using experimental kinetic parameters, such as relaxation lifetime, mobility, and recombination rate constant. These evaluations were in strong agreement with the experimental results [62].

NFAs have significantly enhanced the performance of OPVs, making investigation of their CS processes increasingly critical. Time-resolved spectroscopy is a powerful method for examining the carrier recombination rates and provides key insights into these processes. To date, most studies have focused on the visible region, which primarily detects bound states of charges, such as cations, anions, and singlet (S_n) or triplet (T_n) states confined within molecules. However, these observations are not directly related to the behavior of free charges that contribute to the photocurrent. In contrast, measurements in the infrared region enable the direct observation of weakly bound carriers and free carriers, offering a more accurate assessment of the carrier dynamics that govern solar cell performance. This review summarizes recent findings on the charge separation processes of a representative NFA, ITIC, using transient absorption spectroscopy in the infrared region [63].

In inorganic semiconductors, bound electrons have been reported to cause absorption in the near-infrared region, whereas free carriers result in a broad, structureless absorption in the mid-infrared region [64,65]. Similarly, Yamakata et al. observed comparable characteristic absorptions corresponding to the bound states of electrons in the near-infrared and mid-infrared regions in organic semiconductors, such as ITIC. Fig. 27 shows the time-resolved infrared absorption spectrum of an ITIC single film measured after pump light irradiation. Upon irradiation, a broad peak around 3000 cm^{-1} appears, attributed to the bound state of electrons and holes. Over time, the intensity of this peak decreased, resulting in a broad and flat absorption over the entire mid-infrared region, indicating the presence of free carriers released from their bound states. The intensity of the free carriers increased further when a donor/acceptor interface was formed, where charge separation was enhanced. By analyzing the decay kinetics of the bound electrons and the increase in free carriers, the charge dissociation time constants were determined to be 56 and 23 ps for the neat ITIC and PBDB-T:ITIC blend films, respectively. Thus, transient absorption measurements in the mid-infrared region allow the direct observation of the dissociation process of bound excitons into free carriers.

Time-resolved mid-IR absorption spectroscopy provides detailed insights into the charge separation processes, particularly for NFAs equipped with CN groups as electron-withdrawing sites. The vibrational frequency of the CN group is highly sensitive to changes in the charge density, allowing for precise investigation of both intramolecular and intermolecular charge transfer processes. In the ground state, CN vibrations are observed at 2218 cm^{-1}; however, it was shifted to 2205 cm^{-1} and 2175 cm^{-1} by the photoexcitation (Fig. 28). According to DFT calculations, these shifts correspond to the S_1 state generated by intramolecular electron transfer from the donor to acceptor domain within ITIC and the anionic ITIC formed by intermolecular electron transfer. While it is widely believed that intermolecular charge transfer

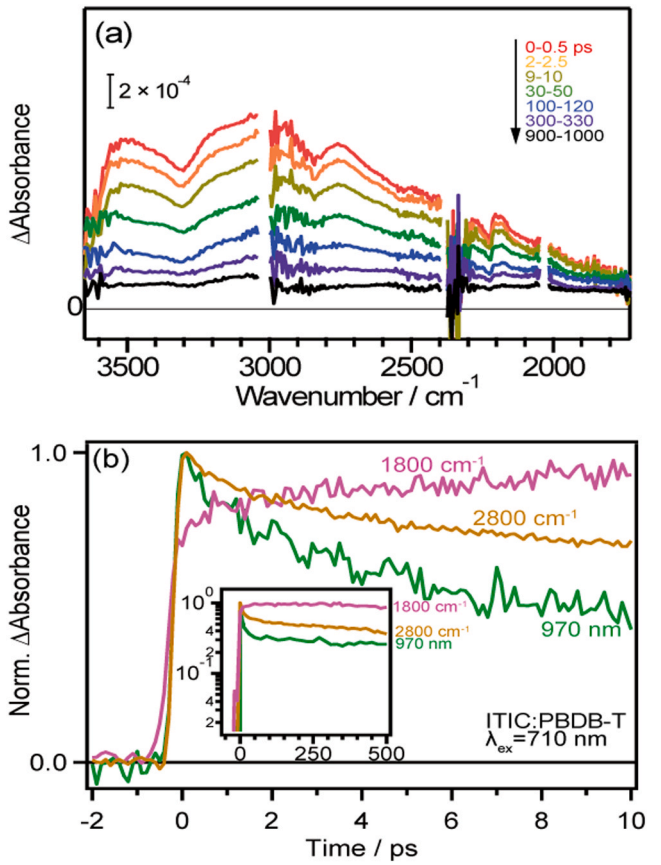

Fig. 27. (a) Transient IR absorption spectra of neat ITIC film after 710-nm laser pulse irradiation. (b) Decay kinetics of the transient absorption of PBDB-T:ITIC blend film. Reprinted from [63]. Copyrights 2024 The Authors. The Royal Chemical Soceity. This publication is licensed under CC-BY-3.0.

takes place at the donor/acceptor interface facilitated by the energy offset, this result demonstrates that intermolecular charge transfer takes place even in neat ITIC films.

Theoretical calculations are valuable tools for analyzing the molecular mechanisms of charge transfer. Molecular dynamics simulations and TDDFT calculations were performed to investigate the conformations and excited states of ITIC in the neat film [63]. It was found that the predominant dimer conformation is J-type, similar to ITIC crystals, although V-type dimers are present at defects such as stacking faults. TD-DFT calculations of representative dimers revealed that low-symmetry V-type dimers shows high absorption energy and significant dipole moment changes upon photoexcitation, whereas low absorption energy with no dipole moment change in the highly symmetric J-type dimers (Fig. 29). This suggests that photoexcitation of the low-symmetry V-type dimer induces intermolecular charge transfer in the neat ITIC films. Additionally, it was found that the dipole moment changes increased with higher excitations beyond the S_1 state, indicating that the absorption of higher-energy photons leads to more efficient intermolecular charge transfer. These findings suggest that direct photoexcitation at the stacking faults, where higher-energy excitations occur, may enhance intermolecular charge transfer more effectively.

Yamakata et al. also reported time-resolved mid-IR absorption spectroscopy of two ITIC-based NFAs, SpiroT-DCI and SpiroF-DCI [52]. As shown in Fig. 30, both NFAs exhibit similar red shifts. Notably, while the relative peak intensities at 2205 and 2175 cm^{-1} varied significantly, the intensity at 2175 cm^{-1} was substantially higher than that at 2205 cm^{-1} for SpiroT-DCI. This suggests a more efficient intermolecular charge separation in SpiroT-DCI than in ITIC. Comparable results were observed for SpiroF-DCI, indicating that intermolecular charge

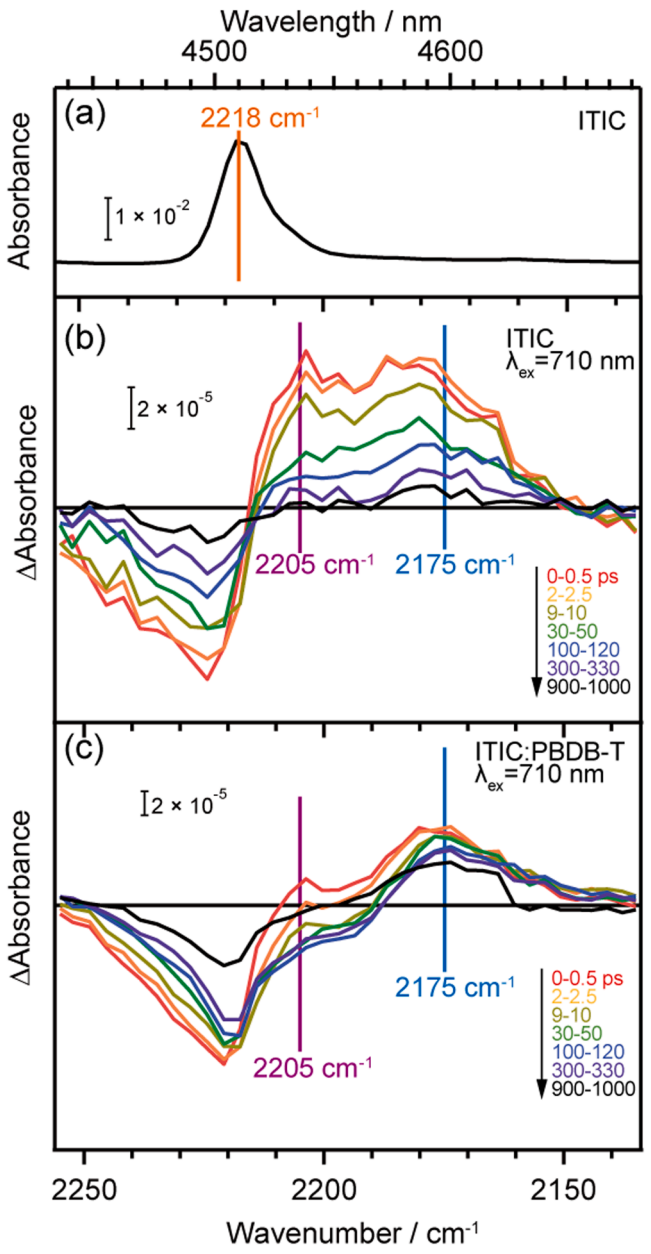

Fig. 28. Vibrational spectra of the CN groups in ITIC. Steady-state FT-IR spectrum of neat ITIC film (a). Transient IR absorption spectra of neat ITIC film (b) and PBDB-T:ITIC blend film (c) irradiated by 710-nm pump pulse. Broad absorption by photocarriers was subtracted to extract the change in CN vibrations. Reprinted from [63]. Copyrights 2024 The Authors. The Royal Chemical Society. This publication is licensed under CC-BY-3.0.

separation also occurred. However, in SpiroF-DCI, the relative peak intensity at 2175 cm^{-1} was much lower than that at 2205 cm^{-1} , indicating a lower frequency of intermolecular charge separation compared to both SpiroT-DCI and ITIC. Based on the intensity ratio of the 2175 to 2205 cm^{-1} peaks, the efficiency of intermolecular charge transfer appears to follow the order: SpiroT-DCI > ITIC > SpiroF-DCI. TR-IR measurements were also performed on blend films incorporating PBDB-T, where only the acceptor molecules (SpiroT-DCI or SpiroF-DCI) were selectively excited using 685 nm laser pulses. As shown in Fig. 29, two positive peaks appeared at 2205 and 2175 cm^{-1} , consistent with the observations of the pristine ITIC films. However, in the PBDB-T: SpiroT-DCI blend films, the decay of the 2205 cm^{-1} peak was notably accelerated, while the lifetime of the 2175 cm^{-1} peak was extended. These results suggest that intermolecular charge separation is more

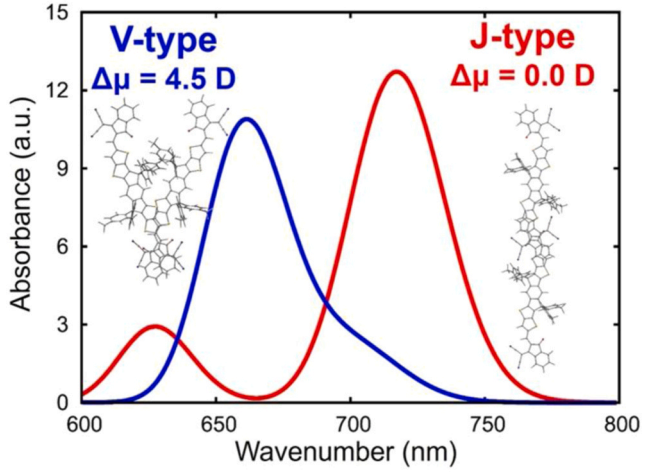

Fig. 29. Calculated absorption spectra of J-type and V-type dimers of ITIC. The dipole moment change on excitation $\Delta\mu$ is also shown.

efficiently promoted in PBDB-T:SpiroT-DCI films at the donor/acceptor interface.

Currently, state-of-the-art OPVs exhibit EQEs approaching 90 %, leading to a J_{SC} of > 27 mA cm^{-2} [66]. This value is comparable to those of the inorganic and perovskite counterparts. However, OPVs suffer from significantly higher voltage loss owing to nonradiative charge recombination (ΔV_{nr}), which is attributed to the significantly smaller oscillator strength of the CT states. Therefore, reducing ΔV_{nr} is the top priority for improving the PCE of the OPVs.

A recent study emphasized the importance of hybridizing the CT state with the LE state to reduce ΔV_{nr} [67]. A hybrid LE–CT state forms when the CT state is energetically very close to the LE state, enhancing emission owing to the so-called the "intensity borrowing" mechanism. Tamai et al. demonstrated a significant reduction in ΔV_{nr} by decreasing the energy offset between the LE and CT states using PTB7-Th as the donor polymer paired with wider-bandgap fullerene and NFAs [68]. It is important to note that the optical bandgaps of all devices were almost the same because they used a common narrow-bandgap donor polymer. They found a steep decrease in ΔV_{nr} with decreasing energy offset (Fig. 31), which was steeper than the general trend predicted by the energy gap law (solid line in the Figure).

Based on transient absorption (TA) measurements, Tamai et al. found that the nonradiative decay rate of the CT state in PTB7-Th:acceptor blends was not sufficiently sensitive to explain the large difference in ΔV_{nr}. Instead, this rapid decrease in ΔV_{nr} was attributed to the large enhancement in the radiative decay rate through LE–CT hybridization, resulting in the enhancement of the photoluminescence quantum yield (PLQY) of the CT states owing to the significantly larger oscillator strength of the LE state. Therefore, minimizing the energy difference between the LE and CT states is crucial for reducing both voltage loss during charge separation and ΔV_{nr}.

Tamai et al. also examined ΔV_{nr} for narrow-bandgap NFA-based OPVs (referred to as h-type OPVs for hole transfer) and compared them to devices where the donor has a narrower bandgap (e-type OPVs, for electron transfer) [70]. Because the charge recombination process does not depend on which (electron transfer or hole transfer) process, charge carriers were generated through, and no significant difference in ΔV_{nr} was observed between the two devices. Both h-type and-type devices can achieve low ΔV_{nr} when the LE and CT states are close in energy.

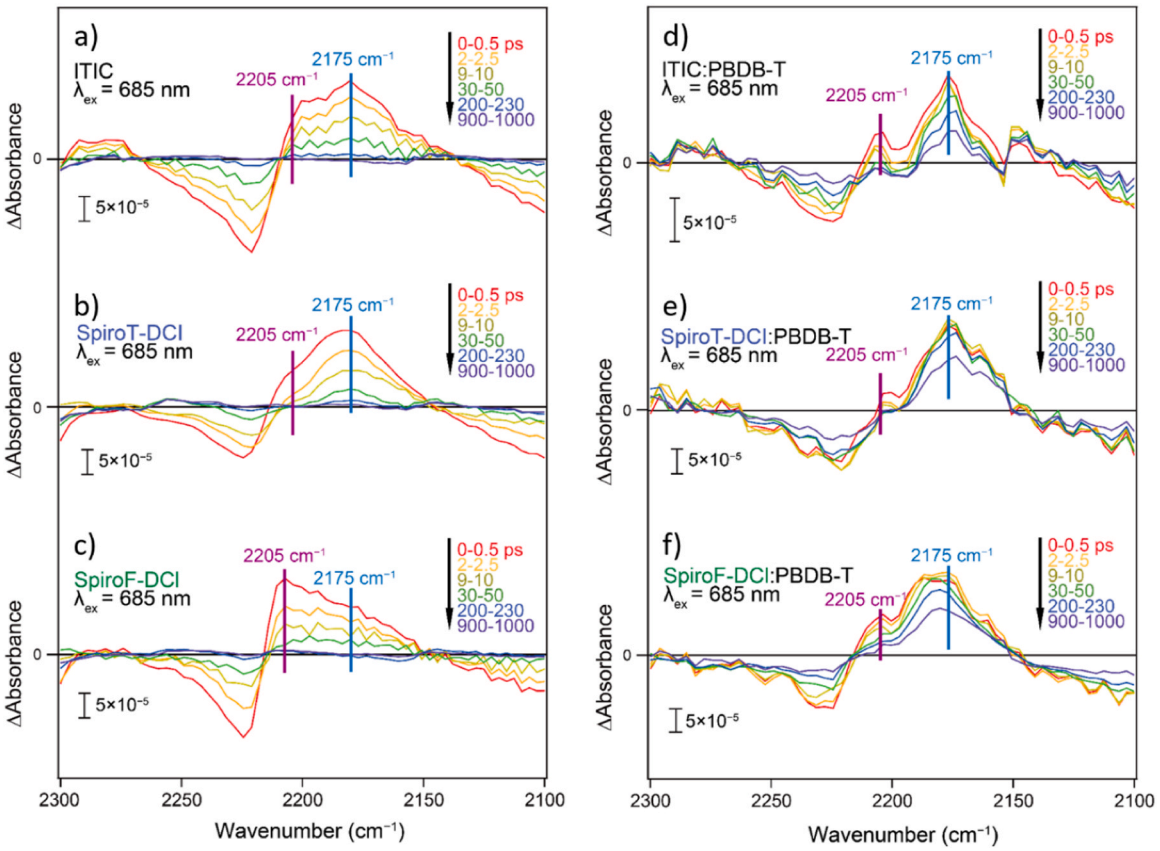

Fig. 30. Differential vibrational spectra of CN groups in NFAs after pump pulse irradiation. Neat ITIC (a), SpiroT-DCI (b), and SpiroF-DCI (c) are photoexcited by a 685 nm pump pulse. The NFA domain in the blend film with PBDB-T is photoexcited by the same 685 nm pump pulse (panels d–f). Adapted from [52]. Copyrights 2024 Wiley-VCH.

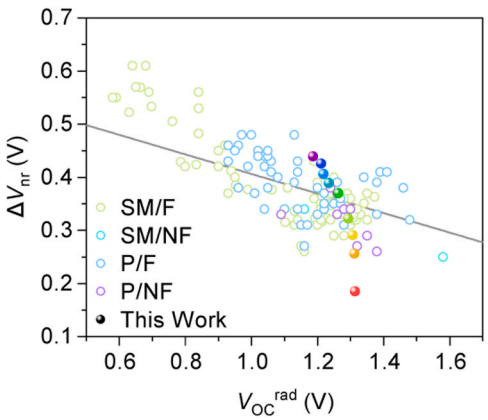

Fig. 31. Nonradiative voltage loss (ΔV_{nr}) as a function of the radiative open-circuit voltage (V_{OC}^{rad}). Previously published data are also shown as open circles. SM, P, F, and NF represent small molecule donor, polymer donor, fullerene acceptor, and NFA respectively. The solid line represents the model trend based on the energy gap law proposed in ref. [69]. Adapted from [68]. Copyrights 2020 The Authors. Wiley-VCH. This publication is licensed under CC-BY-NC-ND 4.0.

However, it is critical to achieve a low ΔV_{nr} while maintaining a high EQE. Tamai *et al.* found that h-type devices tended to exhibit a higher EQE than type devices when the energy offset was small. Therefore, the main advantage of h-type OPVs is their ability to efficiently generate charge carriers with a small energy offset, although the mechanism of charge separation under these conditions remains under investigation. A key priority for future research is to fully elucidate the charge separation mechanism with a small energy offset.

For a long time, it was presumed that a large energy offset (>0.3 eV between the LE and CT states is necessary for efficient charge separation at the D:A interface in OPVs [71]. However, this leads to large voltage loss, resulting in a trade-off between J_{SC} and V_{OC} [72,73].

However, recent studies have shown that efficient charge separation can occur with a significantly smaller energy offset. For instance, PM6:Y6-based OPVs have exhibited a high PCE of over 15 % with a small voltage loss of ~0.55 V and an energy offset of only ~0.1 eV [74]. Tamai et al. investigated the mechanism behind this efficient charge separation in PM6:Y6 blends despite the small energy offset [75]. Fig. 32a shows the TA spectra of the PM6:Y6 blend films. Upon photoexcitation at 800 nm, a large photo-induced absorption (PIA) of Y6 singlet excitons was observed at approximately 930 nm, which then decayed rapidly on picosecond timescales; instead, the PIA of charged species and associated ground state bleaching (GSB) were observed. Strikingly, a positive PIA signal was observed at ~680 nm, owing to the transient electroabsorption (TEA) signal of PM6. When an exciton dissociates into a CT state (i.e., an electron–hole pair), it generates a dipole-like local electric field in the environment. This leads to the addition of a TEA spectrum, which is similar to the first derivative of steady-state absorption, to the TA data [76–78]. The amplitude of the TEA signal increased with increasing separation distance of the electron–hole pair, allowing us to monitor the separation kinetics by tracking the time evolution of the TEA signals.

Fig. 32b shows the time evolution of TA signals monitored at 630 nm (PM6 GSB) and 680 nm (TEA). The TEA signals reached their maximum value slightly after the GSB signals reached their maximum value, indicating that long-range spatial dissociation of CT states occurred on a picosecond timescale. Based on a close inspection of the TA spectra, Tamai et al. revealed that the time evolution of the TEA signals coincided well with the peak shift of the Y6 GSB signals, indicating that the

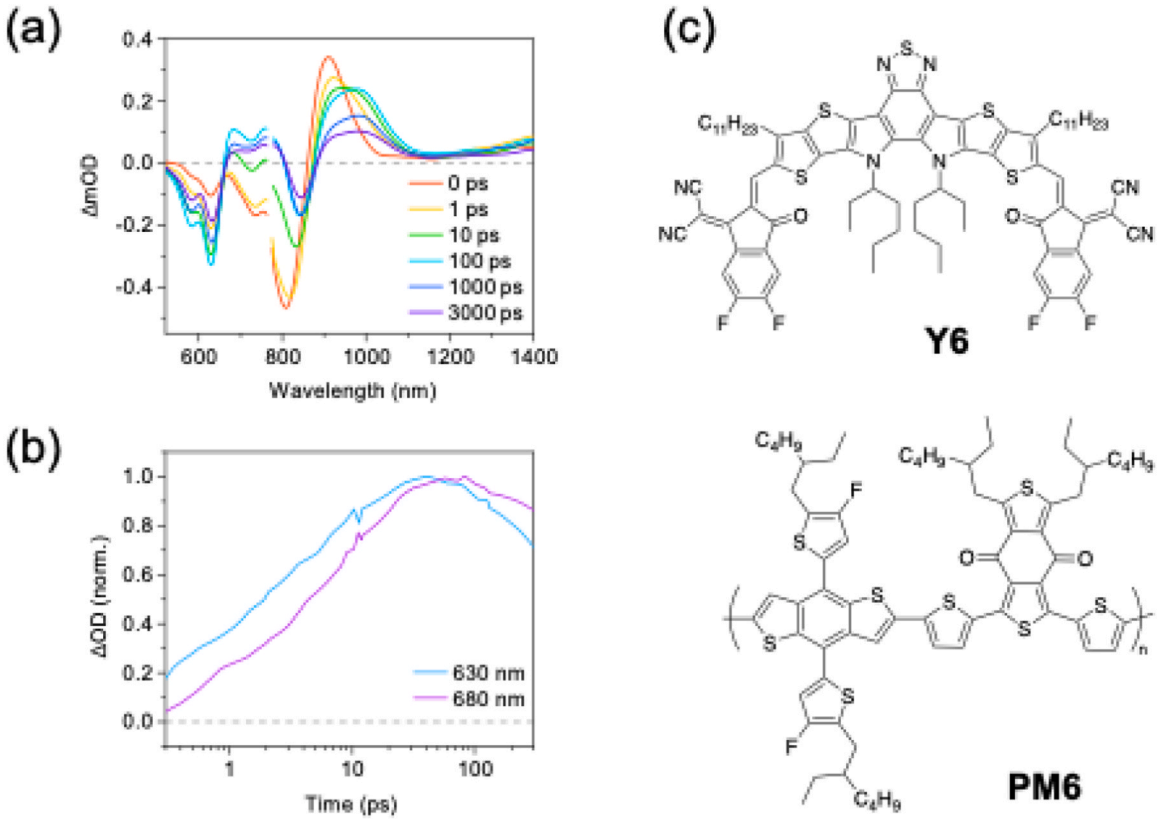

Fig. 32. (a) TA spectra of the PM6:Y6 blend film. The excitation wavelength was 800 nm with a fluence of 1.4 μJ cm^{-2}. (b) Normalized time evolution of the TA signals monitored at 630 nm (PM6 GSB) and 680 nm (PM6 TEA) excited at 800 nm. (c) Chemical structure of Y6 and PM6. Adapted from [75]. Copyrights 2022 The Royal Society of Chemistry.

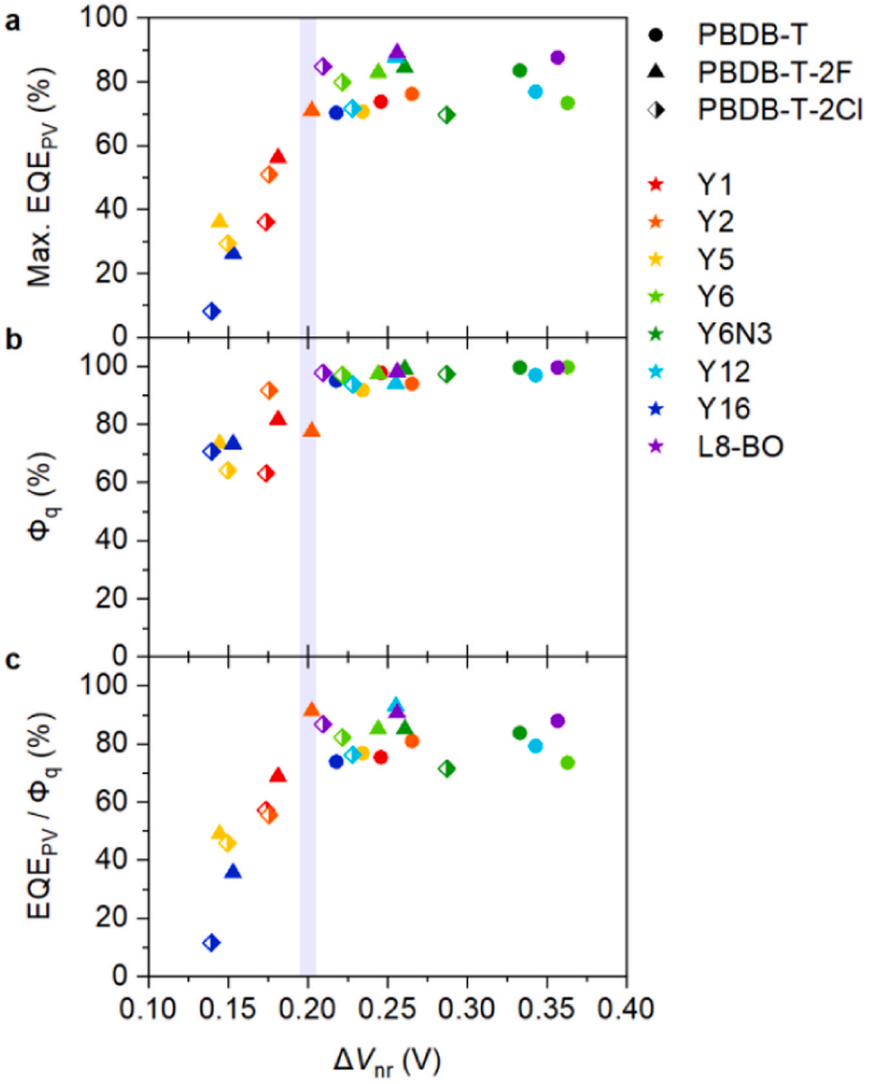

Fig. 33. (a) Maximum EQE$_{PV}$, (b) photoluminescence (PL) quenching yield Φ_q, and (c) EQE$_{PV}$ / Φ_q plotted against ΔV_{nr}. Adapted from [79]. Copyrights 2023 The Authors. The Royal Chemical Society. This publication is licensed under CC-BY-3.0.

slow yet efficient charge dissociation in the PM6:Y6 blend was driven by the downhill energy relaxation of the charges through the cascaded energy landscape formed near the PM6:Y6 interface. The activation energy for the rate constant of charge dissociation was as low as ~4.0–9.4 meV; thus, the charge dissociation efficiency was clearly independent of temperature. As a result, the charges can move away from the PM6:Y6 interface without encountering the activation barrier.

The trade-off between J_{SC} and V_{OC} has been a significant challenge for improving the PCEs of OPVs. While minimizing the energy offset between the LE and CT states is crucial for achieving a high V_{OC}, a very small energy offset often leads to a reduction in J_{SC}, even with high-performance NFAs [70]. Therefore, understanding the extent to which the energy offset can be minimized and the underlying physics of this trade-off is important for optimizing the material design and further enhancing the PCEs.

Tamai et al. found that Y-series OPVs have a clear threshold ΔV_{nr} of 0.2 V, below which the EQEdecreases sharply (Fig. 33a) [79]. This explains why the ΔV_{nr}s of state-of-the-art OPVs remains around 0.2 V, with few reports showing that ΔV_{nr} can exceed this threshold while maintaining a high EQE [52]. According to Marcus theory, the hole transfer rate from the NFA to the donor decreases as the energy offset decreases (Fig. 33b). In contrast, a surprising finding of their results is that the quantum efficiency of long-range spatial dissociation of the CT states also decreases with reduced energy offset (Fig. 33c). They proposed that an activation barrier for charge dissociation still exists even when using an NFA with a large quadrupole moment, and that the quantum efficiency of long-range spatial dissociation depends on the initial separation distance of the CT states. If the initial electron and hole separation after isoenergetic charge transfer is sufficient, barrierless charge dissociation occurs; otherwise, the activation barrier must be overcome, resulting in a lower charge dissociation efficiency. Another notable finding of this study is a clear trade-off between FF and V_{OC}, caused by the reduced charge dissociation efficiency when the energy offset is too small. This trade-off may explain why the ΔV_{nr}s of the state-of-the-art OPVs remained at about 0.2 V.

Although Tamai et al. focused on PBDB-T:Y series blends to minimize the difference in the chemical structure and associated changes in physical properties, the observed trends can be considered general for other NFA systems. Since the threshold energy that can ensure high charge photogeneration quantum efficiencies may depend on the chemical structure, more efforts should be devoted to uncovering the complete details of the charge separation mechanism. Extending a similar study to other D:A systems may reveal what determines the threshold energy and how it can be reduced. Thus, clear material design guidelines can be obtained to enhance the PCE.

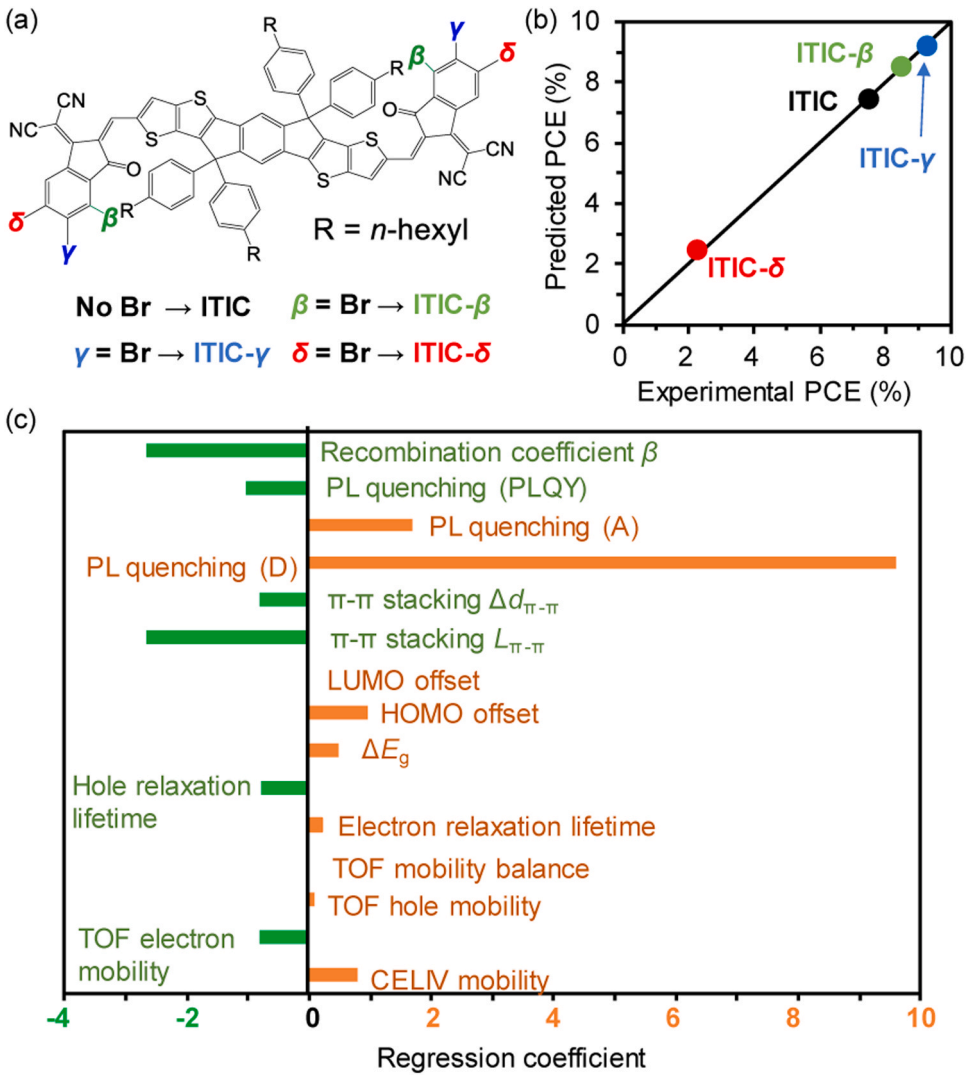

Fig. 34. (a) Chemical structure of brominated ITIC, which includes β, γ, and δ positions. (b) ML regression of experimental (horizontal) and predicted (vertical) PCE. (c) Coefficients of explanatory variables obtained in the ML analysis. Reprinted from [80]. Copyrights 2023 Nature-Springer.

6. Application of machine learning

When the measurements were subjected to another class of NFAs (brominated ITIC, Fig. 34a), the direct correlation between OPV output and kinetic parameters became unclear [80]. To elucidate the intertwining factors that affect OPV performance, machine learning (ML) was performed using 15 experimental parameters, such as mobility, relaxation, recombination rate constant, photoluminescence (PL) quenching, π-π stacking distance, crystallite size, and surface roughness, as the explanatory variables. As shown in Fig. 34b, the regression by ML (an elastic net algorism) shows high accuracy between the experimental and predicted PCE values. By comparing the coefficients, the most important factor for PCE was identified as PL quenching for donor (D) excitation, followed by the recombination rate and crystallite size of π-π stacking (Fig. 34c). As OPV researchers know, device performance-limiting factors vary on a case-by-case basis. This issue can be quantitatively analyzed by collecting the photophysical, optoelectronic, and electrical properties and applying nonlinear analysis methods such as ML.

7. Conclusion

In this review, we summarize novel research on OPVs, with a focus on dynamic excitons. Considering the concept of dynamic excitons, recent advances have been made in prediction and analysis using theoretical calculations, the development of organic semiconductor materials, and the investigation of active layers using various spectroscopic techniques. By integrating these findings and establishing structure-property-function relationships, we can deepen the understanding of carrier generation in OPVs, leading to further improvements in PCEs. In addition, the fundamental principles and insights into dynamic excitons in OPVs are expected to benefit the development of other organic electronic devices that rely on photoexcitation processes, contributing to enhanced device performance.

Declaration of Competing Interest

The authors declare that they have no affiliations with or involvement in any organization or entity with any financial interest in the subject matter or materials discussed in this manuscript.

Acknowledgement

This work was partly supported by a Grant-in-Aid for Transformative Research Areas (A), "Dynamic Exciton" (JSPS KAKENHI Grant Number JP20H05841 for Y.I. and JP20H05833 for H.Y.).

Author Contributions

YI and HY contributed equally to the writing of this paper.

Data availability

No data was used for the research described in the article.

References

[1] J.Q. Zhang, H.S. Tan, X.G. Guo, A. Facchetti, H. Yan, Material insights and challenges for non-fullerene organic solar cells based on small molecular acceptors, Nat. Energy 3 (2018) 720, https://doi.org/10.1038/s41560-018-0181-5.

[2] G. Bianchi, C. Carbonera, L. Ciammaruchi, N. Camaioni, N. Negarville, F. Tinti, G. Forti, A. Nitti, D. Pasini, A. Facchetti, R.M. Pankow, T.J. Marks, R. Po, An anthradithiophene donor polymer for organic solar cells with a good balance between efficiency and synthetic accessibility, Sol. RRL 6 (2022) 2200643, https://doi.org/10.1002/solr.202200643.

[3] Y. Cui, Y. Xu, H. Yao, P. Bi, L. Hong, J. Zhang, Y. Zu, T. Zhang, J. Qin, J. Ren, Z. Chen, C. He, X. Hao, Z. Wei, J. Hou, Single-junction organic photovoltaic cell with 19% efficiency, Adv. Mater. 33 (2021) 2102420, https://doi.org/10.1002/adma.202102420.

[4] L. Zhu, M. Zhang, J. Xu, C. Li, J. Yan, G. Zhou, W. Zhong, T. Hao, J. Song, X. Xue, Z. Zhou, R. Zeng, H. Zhu, C.-C. Chen, R.C.I. MacKenzie, Y. Zou, J. Nelson, Y. Zhang, Y. Sun, F. Liu, Single-junction organic solar cells with over 19% efficiency enabled by a refined double-fibril network morphology, Nat. Mater. 21 (2022) 656, https://doi.org/10.1038/s41563-022-01244-y.

[5] H. Imahori, Y. Kobori, H. Kaji, Manipulation of charge-transfer states by molecular design: perspective from dynamic exciton, Acc. Mater. Res. 2 (2021) 501, https://doi.org/10.1021/accountsmr.1c00045.

[6] H. Tamura, I. Burghardt, Ultrafast charge separation in organic photovoltaics enhanced by charge delocalization and vibronically hot exciton dissociation, J. Am. Chem. Soc. 135 (2013) 16364, https://doi.org/10.1021/ja4093874.

[7] A.A. Bakulin, A. Rao, V.G. Pavelyev, P.H.M. van Loosdrecht, M.S. Pshenichnikov, D. Niedzialek, J. Cornil, D. Beljonne, R.H. Friend, The role of driving energy and delocalized states for charge separation in organic semiconductors, Science 335 (2012) 1340, https://doi.org/10.1126/science.1217745.

[8] K. Vandewal, S. Albrecht, E.T. Hoke, K.R. Graham, J. Widmer, J.D. Douglas, M. Schubert, W.R. Mateker, J.T. Bloking, G.F. Burkhard, A. Sellinger, J. Fréchet, A. Amassian, M.K. Riede, M.D. McGehee, D. Neher, A. Salleo, Efficient charge generation by relaxed charge-transfer states at organic interfaces, Nat. Mater. 13 (2014) 63, https://doi.org/10.1038/nmat3807.

[9] A. Muraoka, M. Fujii, K. Mishima, H. Matsunaga, H. Benten, H. Ohkita, S. Ito, K. Yamashita, Investigations on the charge transfer mechanism at donor/acceptor interfaces in the quest for descriptors of organic solar cell performance, Phys. Chem. Chem. Phys. 20 (2018) 12193, https://doi.org/10.1039/C8CP01253A.

[10] B. Carsten, J.M. Szarko, H.J. Son, W. Wang, L. Lu, F. He, B.S. Rolczynski, S.J. Lou, L.X. Chen, L. Yu, Examining the effect of the dipole moment on charge separation in donor–acceptor polymers for organic photovoltaic applications, J. Am. Chem. Soc. 133 (2011) 20468, 0.1021/ja208642b.

[11] T.L. Bahers, C. Adamo, I. Ciofini, A qualitative index of spatial extent in charge-transfer excitations, J. Chem. Theory Comput. 7 (2011) 2498, https://doi.org/10.1021/ct200308m.

[12] D. Jacquemin, T.L. Bahers, C. Adamo, I. Ciofini, What is the "best" atomic charge model to describe through-space charge-transfer excitations? Phys. Chem. Chem. Phys. (16) (2012) 5383, https://doi.org/10.1039/C2CP40261K.

[13] S. Ikeyama, A. Muraoka, Influence of vibronic interaction of charge transfer excitons in PTB7/BTA-based nonfullerene organic solar cells, J. Chem. Phys. 159 (2023) 044307, https://doi.org/10.1063/5.0150140.

[14] S. Kilina, D. Kilin, S. Tretiak, Light-driven and phonon-assisted dynamics in organic and semiconductor nanostructures, Chem. Rev. 115 (2015) 5929, https://doi.org/10.1021/acs.chemrev.5b00012.

[15] H. Uratani, H. Nakai, Scalable ehrenfest molecular dynamics exploiting the locality of density-functional tight-binding hamiltonian, J. Chem. Theory Comput. 17 (2021) 7384, https://doi.org/10.1021/acs.jctc.1c00950.

[16] S. Ohno, H. Uratani, H. Nakai, Implementation of nonadiabatic molecular dynamics for intersystem crossing based on a time-dependent density-functional tight-binding method, J. Phys. Chem. A 128 (2024) 5999, https://doi.org/10.1021/acs.jpca.4c02422.

[17] H. Uratani, H. Nakai, Nanoscale and real-time nuclear-electronic dynamics simulation study of charge transfer at the donor-acceptor interface in organic photovoltaics, J. Phys. Chem. Lett. 14 (2023) 2292, https://doi.org/10.1021/acs.jpclett.2c03808.

[18] T. Hanada, H. Uratani, H. Nakai, Neutral-to-ionic photoinduced phase transition of tetrathiafulvalene-p-chloranil by electronic and vibrational excitation: a real-time nuclear–electronic dynamics simulation study, J. Chem. Phys. 159 (2023) 054101, https://doi.org/10.1063/5.0159424.

[19] Q. Guo, T. Higashino, R. Adachi, C. Wechwithayakhlung, D. Packwood, A. Yamakata, H. Imahori, Suppression of charge recombination by vertical arrangement of a donor moiety on flat planar dyes for efficient dye-sensitized solar cells, ChemSusChem 17 (2024) e202301661, https://doi.org/10.1002/cssc.202301661.

[20] K. Takahashi, D. Kumagai, N. Yamada, D. Kuzuhara, Y. Yamaguchi, N. Aratani, T. Koganezawa, S. Koshika, N. Yoshimoto, S. Masuo, M. Suzuki, K. Nakayama, H. Yamada, Side-chain engineering in a thermal precursor approach for efficient photocurrent generation, J. Mater. Chem. A 5 (2017) 14003, https://doi.org/10.1039/C7TA04162D.

[21] K. Ohta, K. Tominaga, T. Ikoma, Y. Kobori, H. Yamada, Microscopic structures, dynamics, and spin configuration of the charge carriers in organic photovoltaic solar cells studied by advanced time-resolved spectroscopic methods, Langmuir 38 (2022) 7365, https://doi.org/10.1021/acs.langmuir.2c00290.

[22] B. Kan, M. Li, Q. Zhang, F. Liu, X. Wan, Y. Wang, W. Ni, G. Long, X. Yang, H. Feng, Y. Zuo, M. Zhang, F. Huang, Y. Cao, T.P. Russell, Y. Chen, A series of simple oligomer-like small molecules based on oligothiophenes for solution-processed solar cells with high efficiency, J. Am. Chem. Soc. 137 (2015) 3886, https://doi.org/10.1021/jacs.5b00305.

[23] Q. Zhang, B. Kan, F. Liu, G. Long, X. Wan, X. Chen, Y. Zuo, W. Ni, H. Zhang, M. Li, Z. Hu, F. Huang, Y. Cao, Z. Liang, M. Zhang, T.P. Russell, Y. Chen, Small-molecule solar cells with efficiency over 9%, Nat. Photonics 9 (2015) 35, https://doi.org/10.1038/nphoton.2014.269.

[24] J.A. Love, I. Nagao, Y. Huang, M. Kuik, V. Gupta, C.J. Takacs, J.E. Coughlin, L. Qi, T.S. van der Poll, E.J. Kramer, A.J. Heeger, T.-Q. Nguyen, G.C. Bazan, Silaindacenodithiophene-based molecular donor: morphological features and use in the fabrication of compositionally tolerant, high-efficiency bulk heterojunction solar cells, J. Am. Chem. Soc. 136 (2014) 3597, https://doi.org/10.1021/ja412473p.

[25] J.A. Love, C.M. Proctor, J. Liu, C.J. Takacs, A. Sharenko, T.S. van der Poll, A. J. Heeger, G.C. Bazan, T.-Q. Nguyen, Film morphology of high efficiency solution-processed small-molecule solar cells, Adv. Funct. Mater. 23 (2013) 5019, https://doi.org/10.1002/adfm.201300099.

[26] K. Ohta, S. Tokonami, L. Takahashi, Y. Tamura, H. Yamada, K. Tominaga, Probing charge carrier dynamics in porphyrin-based organic semiconductor thin films by time-resolved THz spectroscopy, J. Phys., Chem. B 121 (2017) 10157, https://doi.org/10.1021/acs.jpcb.7b07025.

[27] K. Ohta, Y. Hiramatsu, K. Takahashi, M. Suzuki, H. Yamada, K. Tominaga, Dynamic behavior of photogenerated charge carriers in diketopyrrolopyrrole-linked tetrabenzoporphyrin-based bulk heterojunction thin films probed with time-resolved terahertz spectroscopy, J. Photochem. Photobio. A 400 (2020) 112693, https://doi.org/10.1016/j.jphotochem.2020.112693.

[28] K. Ohta, Y. Hiramatsu, M. Suzuki, H. Yamada, K. Tominaga, Nature of local charge carrier motions in porphyrin-based bulk heterojunction films revealed by time-resolved optical pump-terahertz probe spectroscopy, Chem. Lett. 50 (2021) 1859, https://doi.org/10.1246/cl.210438.

[29] N. Kudo, K. Uchida, T. Ikoma, K. Takahashi, D. Kuzuhara, M. Suzuki, H. Yamada, D. Kumagai, Y. Yamaguchi, K. Nakayama, Transient photocurrent elucidating carrier dynamics and potential of bulk heterojunction solar cells fabricated by thermal precursor approach, Sol. RRL 2 (2018) 1700234, https://doi.org/10.1002/solr.201700234.

[30] T. Nagatomo, A. Vats, K. Matsuo, S. Oyama, N. Okamoto, M. Suzuki, T. Koganezawa, M. Fuki, S. Masuo, K. Ohta, H. Yamada, Y. Kobori, Nonpolymer organic solar cells: microscopic phonon control to suppress nonradiative voltage loss via charge-separated state, ACS Phys. Chem. Au 3 (2023) 207, https://doi.org/10.1021/acsphyschemau.2c00049.

[31] L. Ma, S. Zhang, J. Wang, Y. Xu, J. Hou, Recent advances in non-fullerene organic solar cells: from lab to fab, Chem. Commun. 56 (2020) 14337, https://doi.org/10.1039/D0CC05528J.

[32] S. Li, L. Zhang, F. Liu, J. Ren, M. Shi, C.-Z. Li, T.P. Russell, H. Chen, An unfused-core-based nonfullerene acceptor enables high-efficiency organic solar cells with excellent morphological stability at high temperatures, Adv. Mater. 30 (2018) 1705208, https://doi.org/10.1002/adma.201705208.

[33] T.-J. Wen, Z.X. Liu, Z. Chen, J.D. Zhou, Z.Q. Shen, Y.Q. Xiao, X.H. Lu, Z.Q. Xie, H. M. Zhu, C.-Z. Li, H.Z. Chen, Simple non-fused electron acceptors leading to efficient organic photovoltaics, Angew. Chem. Int. Ed. 60 (2021) 12964, https://doi.org/10.1002/anie.202101867.

[34] Y.-N. Chen, M. Li, Y. Wang, J. Wang, M. Zhang, Y. Zhou, J. Yang, Y. Liu, F. Liu, Z. Tang, Q. Bao, Z. Bo, A fully non-fused ring acceptor with planar backbone and near-ir absorption for high performance polymer solar cells, Angew. Chem., Int. Ed. 59 (2020) 22714, https://doi.org/10.1002/anie.202010856.

[35] S. Jinnai, Y. Ie, M. Karakawa, T. Aernouts, Y. Nakajima, S. Mori, Y. Aso, Chem. Mater. 28 (2016) 1705.

[36] S. Chatterjee, S. Jinnai, Y. Ie, Nonfullerene acceptors for P3HT-based organic solar cells, J. Mater. Chem. A 9 (2021) 18857, https://doi.org/10.1039/D1TA03219D.

[37] Y. Ie, Y. Okamoto, T. Inoue, S. Tone, T. Seo, Y. Honda, S. Tanaka, S.K. Lee, T. Ohto, R. Yamada, H. Tada, Y. Aso, Highly planar and completely insulated oligothiophenes: effects of π-conjugation on hopping charge transport, J. Phys. Chem. Lett. 10 (2019) 3197, https://doi.org/10.1021/acs.jpclett.9b00747.

[38] Y. Ie, M. Endou, S.K. Lee, R. Yamada, H. Tada, Y. Aso, Completely encapsulated oligothiophenes: synthesis, properties, and single-molecule conductance, Angew. Chem., Int. Ed. 50 (2011) 11980, https://doi.org/10.1002/anie.201104700.

[39] S. Jinnai, K. Murayama, K. Nagai, M. Mineshita, K. Kato, A. Muraoka, A. Yamakata, A. Saeki, Y. Kobori, Y. Ie, Effects of the rigid and sterically bulky structure of non-fused nonfullerene acceptors on transient photon-to-current dynamics, J. Mater. Chem. A 10 (2022) 20035, https://doi.org/10.1039/D2TA02604J.

[40] S. Jinnai, N. Shimohara, K. Ishikawa, K. Hama, Y. Iimuro, T. Washio, Y. Watanabe, Y. Ie, Green-light wavelength-selective organic solar cells for agrivoltaics: dependence of wavelength on photosynthetic rate, Faraday Discuss. 250 (2024) 220, https://doi.org/10.1039/D3FD00141E.

[41] T. Umeyama, K. Igarashi, Y. Tamai, T. Wada, T. Takeyama, D. Sasada, K. Ishida, T. Koganezawa, S. Ohtani, K. Tanaka, H. Ohkita, H. Imahori, Prolongation of the singlet exciton lifetime of nonfullerene acceptor films by the replacement of the central benzene core with naphthalene, Sustain. Energy Fuels 5 (2021) 2028, https://doi.org/10.1039/D0SE01861A.
[42] T. Umeyama, T. Wada, K. Igarashi, K. Kato, A. Yamakata, T. Takeyama, Y. Sakamoto, Y. Tamai, H. Ohkita, K. Ishida, T. Koganezawa, S. Ohtani, K. Tanaka, H. Imahori, Effect of terminal-group halogenation of naphthalene-based nonfullerene acceptors on their film structure and photophysical and photovoltaic properties, ACS Appl. Energy Mater. 4 (2021) 14022, https://doi.org/10.1021/acsaem.1c02816.
[43] T. Umeyama, M. Kubota, H. Zhang, R. Adachi, A. Yamakata, T. Koganezawa, H. Imahori, Development of non-fullerene acceptors with π-extended central unit for organic photovoltaic devices, J. Photopolym. Sci. Technol. 37 (2024) 197, https://doi.org/10.2494/photopolymer.37.197.
[44] M. Knupfer, Exciton binding energies in organic semiconductors, Appl. Phys. A 77 (2003) 623, https://doi.org/10.1007/s00339-003-2182-9.
[45] Y. Zhu, F. Zhao, W. Wang, Y. Li, S. Zhang, Y. Lin, Exciton binding energy of non-fullerene electron acceptors, Adv. Energy Sustain. Res. 3 (2022) 2100184, https://doi.org/10.1002/aesr.202100184.
[46] P.J. Leenaers, A. Maufort, M.M. Wienk, R.A.J. Janssen, Impact of π-conjugated linkers on the effective exciton binding energy of diketopyrrolopyrrole–dithienopyrrole copolymers, J. Phys. Chem. C. 124 (2020) 27403, https://doi.org/10.1021/acs.jpcc.0c08768.
[47] J. Zhang, J. Guan, Y. Zhang, S. Qin, Q. Zhu, X. Kong, Q. Ma, X. Li, L. Meng, Y. Yi, J. Zheng, Y. Li, Direct observation of increased free carrier generation owing to reduced exciton binding energies in polymerized small-molecule acceptors, J. Phys. Chem. Lett. 13 (2022) 8816, https://doi.org/10.1021/acs.jpclett.2c02337.
[48] T. Li, K. Wang, G. Cai, Y. Li, H. Liu, Y. Jia, Z. Zhang, X. Lu, Ye Yang, Y. Lin, Asymmetric glycolated substitution for enhanced permittivity and ecocompatibility of high-performance photovoltaic electron acceptor, JACS Au 1 (2021) 1733, https://doi.org/10.1021/jacsau.1c00306.
[49] L. Zhu, Y. Yi, Z. Wei, Exciton binding energies of nonfullerene small molecule acceptors: implication for exciton dissociation driving forces in organic solar cells, J. Phys. Chem. C. 122 (2018) 22309, https://doi.org/10.1021/acs.jpcc.8b07197.
[50] Z.A. Lan, G.G. Zhang, X. Chen, Y.F. Zhang, K.A.I. Zhang, X.C. Wang, Reducing the exciton binding energy of donor–acceptor-based conjugated polymers to promote charge-induced reactions, Angew. Chem. Int. Ed. 58 (2019) 10236, https://doi.org/10.1002/anie.201904904.
[51] H. Mori, S. Jinnai, Y. Hosoda, A. Muraoka, K.-i Nakayama, A. Saeki, Y. Ie, A Dibenzo[g,p]chrysene-based organic semiconductor with small exciton binding energy via molecular aggregation, Angew. Chem. Int. Ed. 63 (2024) e202409964, https://doi.org/10.1002/anie.202409964.
[52] K. Wang, S. Jinnai, T. Urakami, H. Sato, M. Higashi, S. Tsujimura, Y. Kobori, R. Adachi, A. Yamakata, Y. Ie, Nonfullerene acceptors bearing spiro-substituted bithiophene units in organic solar cells: tuning the frontier molecular orbital distribution to reduce exciton binding energy, Angew. Chem. Int. Ed. 63 (2024) e202412691, https://doi.org/10.1002/anie.202412691.
[53] A. Sugie, K. Nakano, K. Tajima, I. Osaka, H. Yoshida, Dependence of exciton binding energy on bandgap of organic semiconductors, J. Phys. Chem. Lett. 14 (2023) 11412, https://doi.org/10.1021/acs.jpclett.3c02863.
[54] S.A. Abd-Rahman, T. Yamaguchi, S. Kera, H. Yoshida, Sample-shape dependent energy levels in organic semiconductors, Phys. Rev. B 106 (2022) 075303, https://doi.org/10.1103/PhysRevB.106.075303.
[55] D.A. Vithanage, A. Devižis, V. Abramavičius, Y. Infahsaeng, D. Abramavičius, R.C. I. MacKenzie, P.E. Keivanidis, A. Yartsev, D. Hertel, J. Nelson, V. Sundström, V. Gulbinas, Visualizing charge separation in bulk heterojunction organic solar cells, Nat. Commun. 4 (2013) 2334, https://doi.org/10.1038/ncomms3334.
[56] J.-T. Shieh, C.-H. Liu, H.-F. Meng, S.-R. Tseng, Y.-C. Chao, S.F. Horng, The effect of carrier mobility in organic solar cells, J. Appl. Phys. 107 (2010) 084503, https://doi.org/10.1063/1.3327210.
[57] A. Saeki, Evaluation-oriented exploration of photo energy conversion systems: from fundamental optoelectronics and material screening to the combination with data science, Polym. J. 52 (2020) 1307, https://doi.org/10.1038/s41428-020-00399-2.
[58] A. Melianas, M. Kemerink, Photogenerated charge transport in organic electronic materials: experiments confirmed by simulations, Adv. Mater. 31 (2019) 1806004, https://doi.org/10.1002/adma.201806004.
[59] Y. Shimata, M. Ide, M. Tashiro, M. Katouda, Y. Imamura, A. Saeki, Charge dynamics at heterojunction between face-on/edge-on PCPDTBT and PCBM bilayer: interplay of donor/acceptor distance and local charge carrier mobility, J. Phys. Chem. C. 120 (2016) 17887, https://doi.org/10.1021/acs.jpcc.6b04827.
[60] F. Hamada, A. Saeki, Mobility relaxation of holes and electrons in polymer: fullerene and polymer: non-fullerene acceptor solar cells, ChemSusChem 14 (2021) 3528, https://doi.org/10.1002/cssc.202100566.
[61] W. Zhu, A.P. Spencer, S. Mukherjee, J.M. Alzola, V.K. Sangwan, S.H. Amsterdam, S. M. Swick, L.O. Jones, M.C. Heiber, A.A. Herzing, G. Li, C.L. Stern, D. M. DeLongchamp, K.L. Kohlstedt, M.C. Hersam, G.C. Schatz, M.R. Wasielewski, L. X. Chen, A. Facchetti, T.J. Marks, Crystallography, morphology, electronic structure, and transport in non-fullerene/non-indacenodithienothiophene polymer: Y6 solar cells, J. Am. Chem. Soc. 142 (2020) 14532, https://doi.org/10.1021/jacs.0c05560.
[62] S. Li, F. Hamada, R. Nishikubo, A. Saeki, Quantifying the optimal thickness in polymer: fullerene solar cells from the analysis of charge transport dynamics and photoabsorption, Sustain. Energy Fuels 6 (2022) 756, https://doi.org/10.1039/D1SE01228B.
[63] A. Yamakata, K. Kato, T. Urakami, S. Tsujimura, K. Murayama, M. Higashi, H. Sato, Y. Kobori, T. Umeyama, H. Imahori, Boosting charge separation in organic photovoltaics: unveiling dipole moment variations in excited non-fullerene acceptor layers, Chem. Sci. 15 (2024) 12686, https://doi.org/10.1039/D4SC00917G.
[64] J.I. Pankove, Optical Processes in Semiconductors, Dover, 1975.
[65] A. Yamakata, M. Kawaguchi, N. Nishimura, T. Minegishi, J. Kubota, K. Domen, Behavior and energy states of photogenerated charge carriers on Pt- or CoO_x-loaded $LaTiO_2N$ photocatalysts: time-resolved visible to mid-infrared absorption study, J. Phys. Chem. C. 118 (2014) 23897, https://doi.org/10.1021/jp508233z.
[66] Y. Tamai, What's next for organic solar cells? The frontiers and challenges, Adv. Energy Sustain. Res. 4 (2023) 2200149, https://doi.org/10.1002/aesr.202200149.
[67] F.D. Eisner, M. Azzouzi, Z. Fei, X. Hou, T.D. Anthopoulos, T.J.S. Dennis, M. Heeney, J. Nelson, Hybridization of local exciton and charge-transfer states reduces nonradiative voltage losses in organic solar cells, J. Am. Chem. Soc. 141 (2019) 6362–6374, https://doi.org/10.1021/jacs.9b01465.
[68] T. Saito, S. Natsuda, K. Imakita, Y. Tamai, H. Ohkita, Role of energy offset in nonradiative voltage loss in organic solar cells, Sol. RRL 4 (2020) 2000255, https://doi.org/10.1002/solr.202000255.
[69] J. Benduhn, K. Tvingstedt, F. Piersimoni, S. Ullbrich, Y. Fan, M. Tropiano, K. A. McGarry, O. Zeika, M.K. Riede, C.J. Douglas, S. Barlow, S.R. Marder, D. Neher, D. Spoltore, K. Vandewal, Intrinsic non-radiative voltage losses in fullerene-based organic solar cells, Nat. Energy 2 (2017) 17053, https://doi.org/10.1038/nenergy.2017.53.
[70] T. Saito, S. Natsuda, R. Shirouchi, K. Imakita, K. Kohzuki, Y. Tamai, Intrinsic advantage of fused-ring nonfullerene acceptor-based organic solar cells to reduce voltage loss, Phys. Status Solidi A 220 (2023) 2300121, https://doi.org/10.1002/pssa.202300121.
[71] Y. Tamai, Charge generation in organic solar cells: journey toward 20% power conversion efficiency, Aggregate 3 (2022) e280, https://doi.org/10.1002/agt2.280.
[72] W. Li, K.H. Hendriks, A. Furlan, M.M. Wienk, R.A.J. Janssen, High quantum efficiencies in polymer solar cells at energy losses below 0.6 eV, J. Am. Chem. Soc. 137 (2015) 2231, https://doi.org/10.1021/ja5131897.
[73] K. Kawashima, Y. Tamai, H. Ohkita, I. Osaka, K. Takimiya, High-efficiency polymer solar cells with small photon energy loss, Nat. Commun. 6 (2015) 10085, https://doi.org/10.1038/ncomms10085.
[74] J. Yuan, Y.Q. Zhang, L.Y. Zhou, G.C. Zhang, H.L. Yip, T.K. Lau, X.H. Lu, C. Zhu, H. J. Peng, P.A. Johnson, M. Leclerc, Y. Cao, J. Ulanski, Y.F. Li, Y. Zou, Single-junction organic solar cell with over 15% efficiency using fused-ring acceptor with electron-deficient core, Joule 3 (2019) 1140, https://doi.org/10.1016/j.joule.2019.01.004.
[75] S. Natsuda, T. Saito, R. Shirouchi, Y. Sakamoto, T. Takeyama, Y. Tamai, H. Ohkita, Cascaded energy landscape as a key driver for slow yet efficient charge separation with small energy offset in organic solar cells, Energy Environ. Sci. 15 (2022) 1545, https://doi.org/10.1039/D1EE03565G.
[76] S. Gélinas, A. Rao, A. Kumar, S.L. Smith, A.W. Chin, J. Clark, T.S. van der Poll, G. C. Bazan, R.H. Friend, Ultrafast long-range charge separation in organic semiconductor photovoltaic diodes, Science 343 (2014) 512, https://doi.org/10.1126/science.1246249.
[77] Y. Tamai, Y. Fan, V.O. Kim, K. Ziabrev, A. Rao, S. Barlow, S.R. Marder, R.H. Friend, S.M. Menke, Ultrafast long-range charge separation in nonfullerene organic solar cells, ACS Nano 11 (2017) 12473, https://doi.org/10.1021/acsnano.7b06575.
[78] Y. Tamai, Y. Murata, S. Natsuda, Y. Sakamoto, How to interpret transient absorption data?: an overview of case studies for application to organic solar cells, Adv. Energy Mater. 14 (2024) 2301890, https://doi.org/10.1002/aenm.202301890C.
[79] Y. Tamai, R. Shirouchi, T. Saito, K. Kohzuki, S. Natsuda, Role of the energy offset in the charge photogeneration and voltage loss of nonfullerene acceptor-based organic solar cells, J. Mater. Chem. A 11 (2023) 17581, https://doi.org/10.1039/D3TA01928D.
[80] S. Li, R. Nishikubo, T. Wada, T. Umeyama, H. Imahori, A. Saeki, Unraveling complex performance-limiting factors of brominated ITIC derivative: PM6 organic solar cells by using time-resolved measurements, Polym. J. 55 (2023) 463, https://doi.org/10.1038/s41428-022-00704-1.

Prof. Yutaka Ie received his PhD from Osaka University in 2000 under the supervision of Prof. Shinji Murai. After working at Sumitomo Pharamaceuticals Co., Ltd. as a research scientist for three years, he was appointed assistant professor of Prof. Yoshio Aso group at The Institute of Scientific and Industrial Research, Osaka University in 2003, and associate professor in 2009. In 2019, he was promoted to full professor. His current research focuses on the development of novel organic molecules for organic electronics and single-molecule electronics.

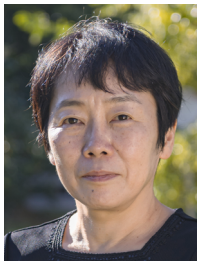

Hiroko Yamada received her Ph.D. degree in 1992 from Kyoto University, under the guidance of Prof. Kazuhiro Maruyama and Prof. Atsuhiro Osuka. In 2003, she was promoted as an associate professor in the group of Prof. Noboru Ono in Graduate School of Science and Engineering, Ehime University, and moved to Graduate School of Materials Science, Nara Institute of Science and Technology (NAIST) in 2011. She was promoted to a full professor at NAIST in 2012 and moved to Institute for Chemical Research (ICR), Kyoto University in 2023. In 2006–2010, she was a researcher of PRESTO, JST. Her current research interest is development of small molecular organic electronic materials for the morphology control in thin films using precursor approach.